4. Cooling and trapping with laser light

4.1 Mechanical effects of light I: The scattering force

- Basic Scattering force
- Zeeman slower
- Doppler cooling
- Polarization gradient cooling
- Radiation pressure trapping
  - Magneto Optical Trap
- Coherent population trapping

4.2 Mechanical effects of light II: The dipole force

- Dressed state potentials
- Dipole traps
  - Optical Tweezers
  - RF trap
- Optical lattices

4.3 Controlling Atoms with Light
Controlling Light with Atoms

- Coherent population transfer (STIRAP)
- Electromagnetically Induced Transparency (EIT)
- Slow Light, Stopping Light

Experimental Methods

Roadmap to BEC with an atomic gas

Laser cooling, magnetic trapping, evaporative cooling

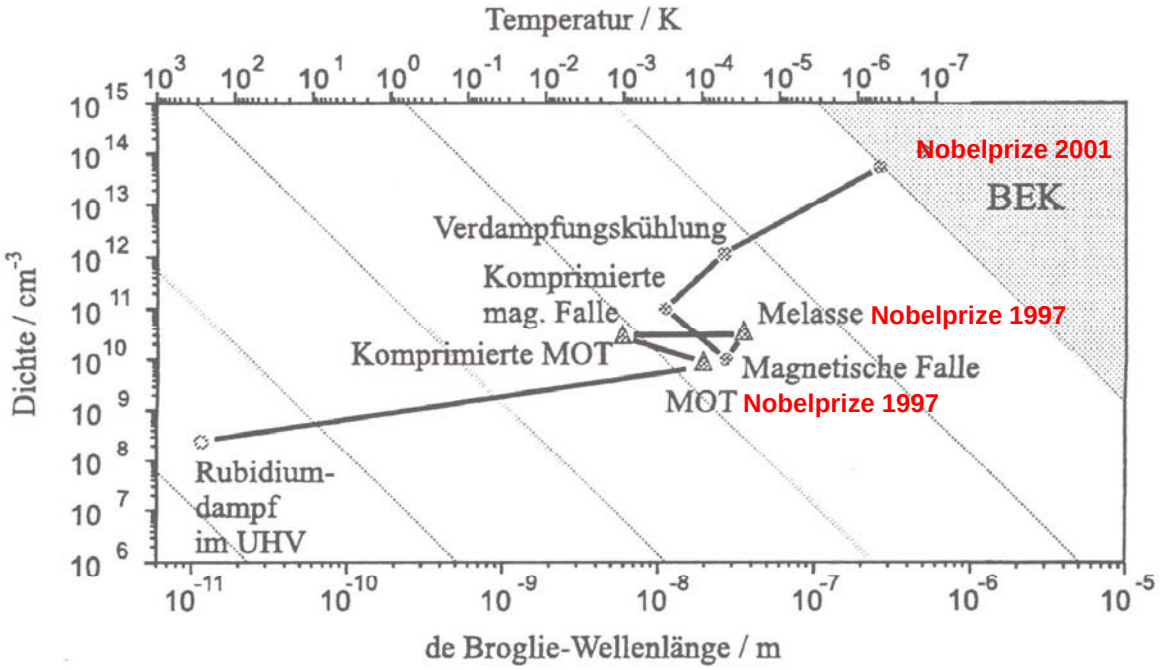

Experimental Methods
Cold Atoms

Laser Cooling
Neutral atoms can be cooled by interacting with monochromatic light (~thermal equilibrium with the light)

- Temperature 1mK ⇨ 1μK
- Velocity 0.5m/s ⇨1mm/s
- deBroglie wavelength 10nm ⇨500nm
- Typical samples 10^8 atoms @ 10^{11} atoms/cm^3

Magnetic Trapping
Neutral atoms can be magnetically trapped U=-μB
1Gauss ~ 67 μK for a magnetic moment $\mu = \mu_B$

BEC
Cooling in a magnetic trap by removing the hottest atoms and thermal equilibration (evaporative cooling)

- Typical samples >10^5 atoms @ 10^{14} atoms/cm^3
- Temperature <1μK
- deBroglie wavelength >1μm

Kalte Atome
Basics

Basic relations

	E [eV]	v [cm s^{-1}]	λ [Å]	h [cm]
E [eV]		$5.182\ 10^{-13}\ A\ v^2$	$\frac{0.0825}{A\ \lambda^2}$	$1.017\ 10^{-9}\ A\ h$
v [cm s^{-1}]	$1.389\ 10^6 \sqrt{\frac{E}{A}}$		$\frac{3.990\ 10^5}{A\ \lambda}$	$44.29\ \sqrt{h}$
λ [Å]	$\frac{0.2873}{\sqrt{E\ A}}$	$\frac{3.990\ 10^5}{A\ v}$		$\frac{9008.6}{A\ \sqrt{h}}$
h [cm]	$9.836\ 10^8\ \frac{E}{A}$	$5.097\ 10^{-4}\ v^2$	$\frac{8.115\ 10^7}{A^2\ \lambda^2}$	

$$t = 0.04515\ \sqrt{h}$$

4.1 Mechanical effects of light I: The scattering force

Basic Scattering force
Zeeman slower
Doppler cooling
Polarization gradient cooling
Radiation pressure trapping
Magneto Optical Trap
Coherent population trapping

Mechanical Effects of Light

the scattering force

Scattering of a photon by an atom

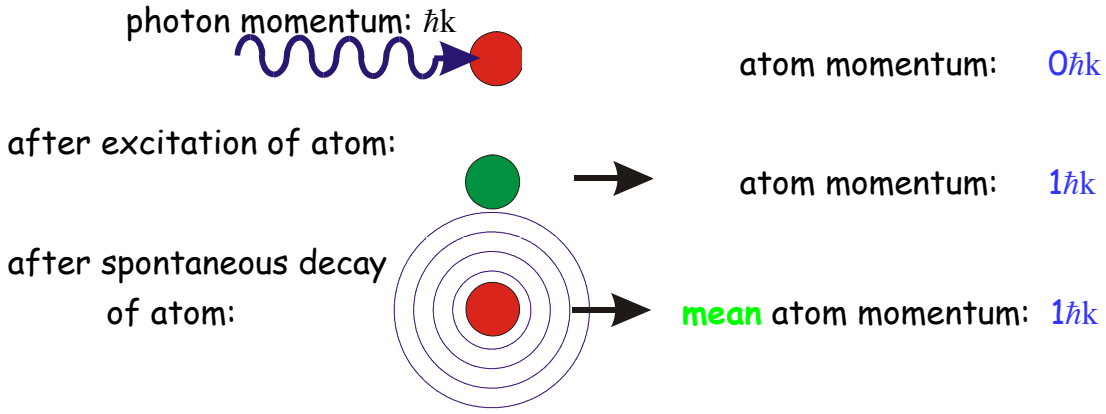

Mean force on atom:

$$F = \frac{dp}{dt} \approx \frac{\Delta p}{\Delta t} = \hbar k \Gamma \rho_{22} = \hbar k \frac{\Gamma}{2} \frac{I/I_0}{1 + I/I_0 + (2\frac{\omega_L - \omega_a - \vec{k}\vec{v}}{\Gamma})^2}$$

typical forces on the atom can lead to accelerations of 10^4-10^6 m/s^2

Interaction with Light

Quantum Mechanics:
Optical Bloch Equation

A basic introduction can be found in the first two chapters of:
R. Laudon: Quantum Theory of Light (Oxford Uni. Press)

without radiation damping

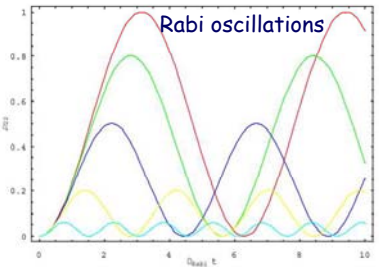

with radiation damping

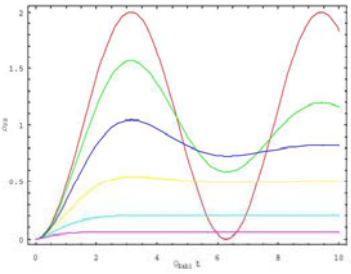

Rate equations and Einstein relations

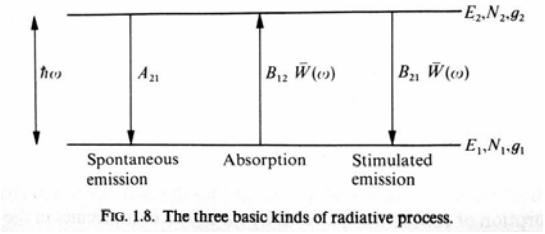

FIG. 1.8. The three basic kinds of radiative process.

$$\frac{g_1}{g_2} B_{12} = B_{21}$$
$$\frac{\hbar\omega^3}{\pi^2 c^3} B_{21} = A_{21}$$
$$A_{21} = \frac{\hbar\omega_0^3 g_1}{\pi^2 c^3 g_2} B_{21} = \frac{e\omega_0^3 g_1}{3\pi\varepsilon_0 \hbar c^3 g_2} |D_{12}|^2$$

Line shape for:
Ω_{rabi} = 10γ, 4γ, 2γ, 1γ, 0.1γ,

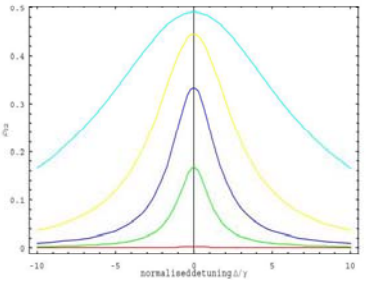

Power broadening illustrated by normalized line shape for:
Ω_{rabi} = 10γ, 4γ, 2γ, 1γ, 0.1γ,

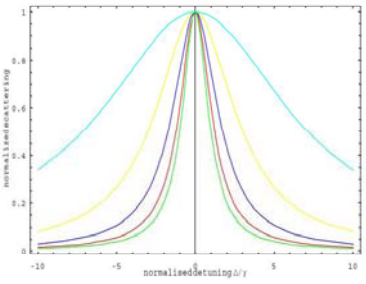

Zeeman Slowing

W. Phillips, H. Metcalf PRL **48** p569 (1982)

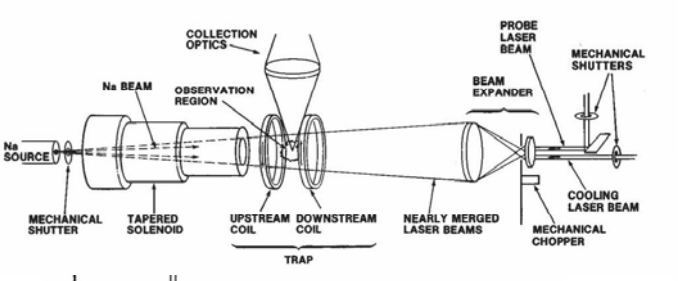

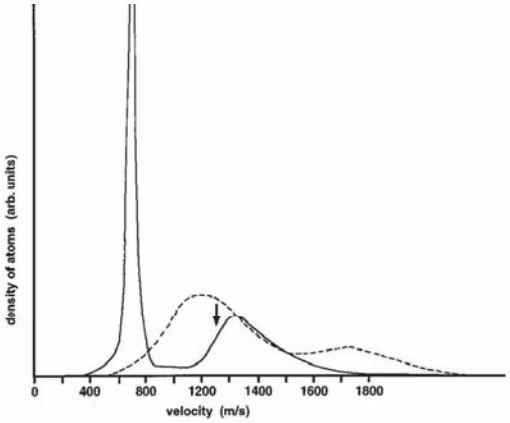

FIG. 5. Velocity distribution before (dashed) and after (solid) Zeeman cooling. The arrow indicates the highest velocity resonant with the slowing laser. (The extra bump at 1700 m/s is from $F=1$ atoms, which are optically pumped into $F=2$ during the cooling process.)

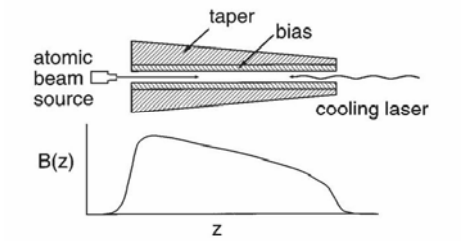

FIG. 4. Upper: Schematic representation of a Zeeman slower. Lower: Variation of the axial field with position.

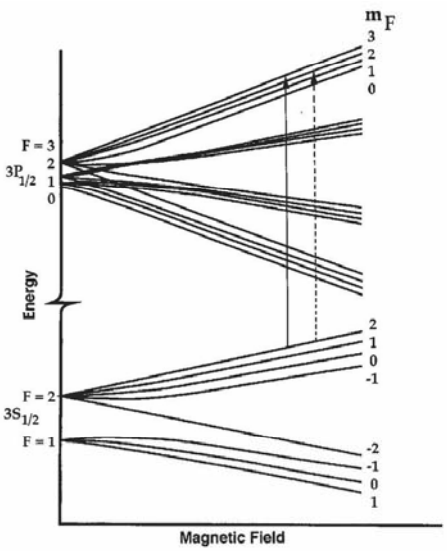

FIG. 6. Energy levels of Na in a magnetic field. The cycling transition used for laser cooling is shown as a solid arrow, and one of the nearly forbidden excitation channels leading to undesirable optical pumping is shown dashed.

Cold Atoms
laser cooling

Atom in counter propagating laser field: optical molasses

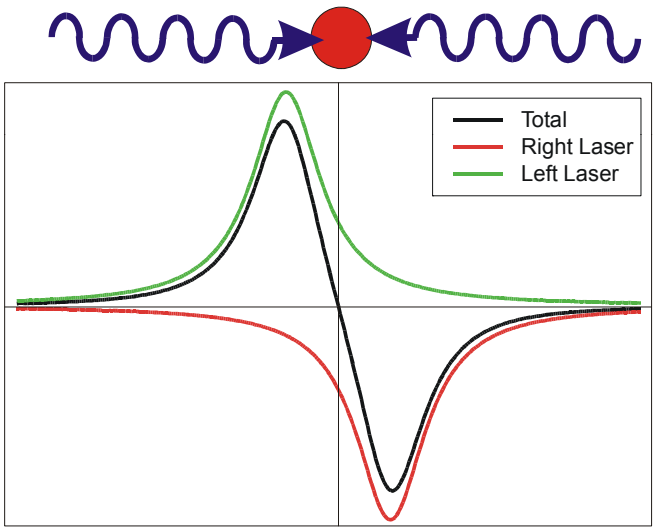

Close to velocity zero: force is linear in velocity

$$F=-\alpha v$$

For a detuning

$$\delta=\omega_{laser}-\omega_{atom}<0$$

(red from resonance) $\alpha>0$ and the force is a damping force

Heating due to randomness of the photon scattering
typical temperature: $k_B T=\hbar\Gamma/2$ (Doppler limit)
140 μK for Γ=5 MHz

Doppler Molasses

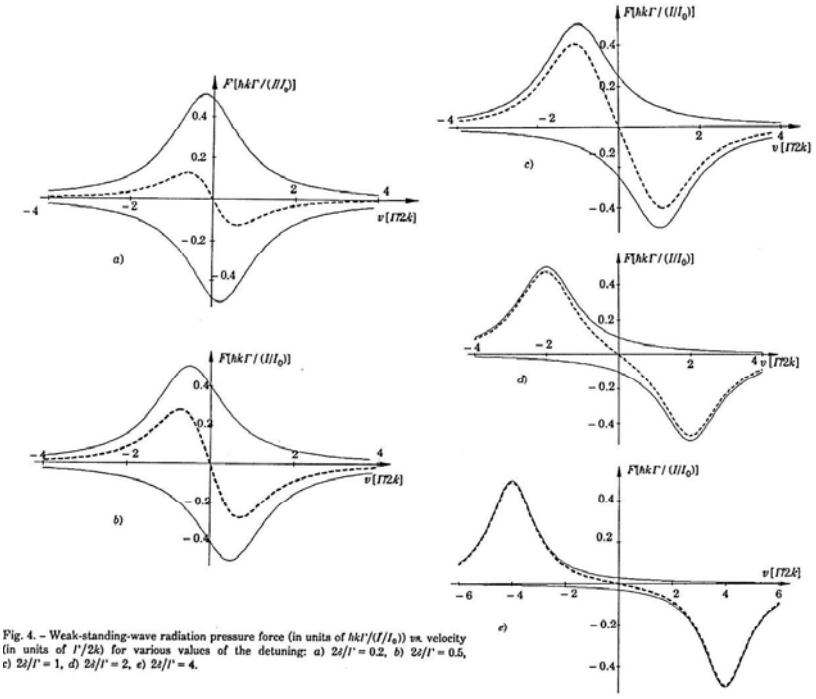

Fig. 4. – Weak-standing-wave radiation pressure force (in units of $\hbar k\Gamma/(I/I_0)$) vs. velocity (in units of $\Gamma/2k$) for various values of the detuning: a) $2\delta/\Gamma=0.2$, b) $2\delta/\Gamma=0.5$, c) $2\delta/\Gamma=1$, d) $2\delta/\Gamma=2$, e) $2\delta/\Gamma=4$.

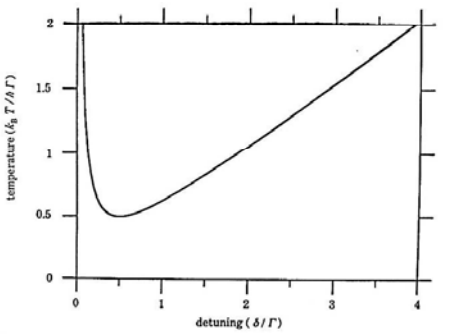

Fig. 3. – Equilibrium temperature for laser cooling at low intensity as a function of laser detuning.

cooling limit for Doppler cooling:

$$k_B T=\frac{\hbar\Gamma}{4}\frac{1+\frac{I}{I_0}+\left(\frac{2\delta}{\Gamma}\right)^2}{\frac{2\delta}{\Gamma}}$$

for $I/I_0 \ll 1$ and $2\delta/\Gamma=1$

$$k_B T=\frac{\hbar\Gamma}{2}$$

Measuring Temperature

release and recapture

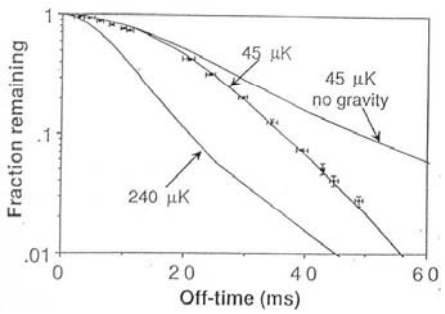

time of flight

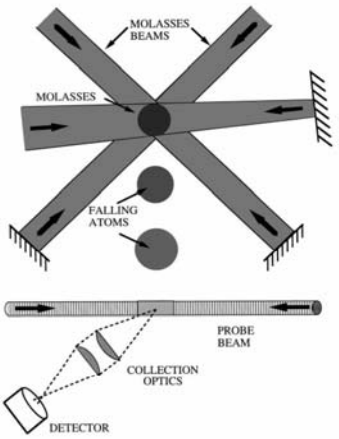

FIG. 15. Time-of-flight method for measuring laser cooling temperatures.

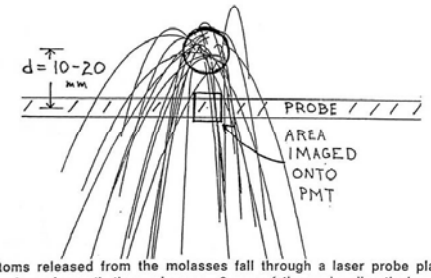

Atoms released from the molasses fall through a laser probe placed 1 - 2 cm beneath the molasses. 8 mm of the probe directly beneath the molasses are imaged onto a photomultiplier and the counts collected by a signal averager.

Molasses Experiment

life time

Lett et al. JOSA B6 p2084 (1989)

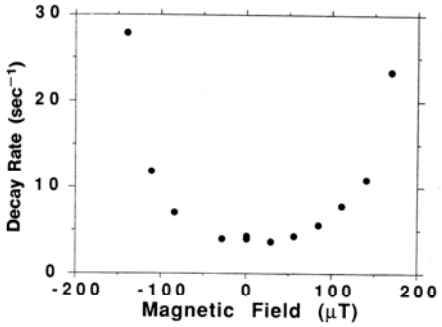

Fig. 21. Molasses decay rate versus magnetic field. $\Delta = -2.5\Gamma$; power, 10 mW.

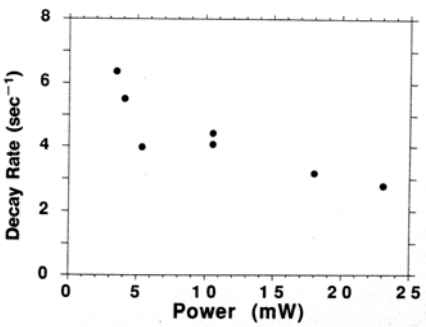

Fig. 22. Molasses decay rate versus laser power. $\Delta = -2.5\Gamma$.

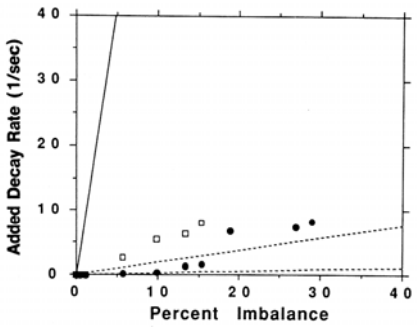

Fig. 10. Added decay rate of the molasses due to imbalance in one pair of beams versus the percent intensity imbalance. The filled circles and open boxes indicate two independent experimental data sets. The solid curve indicates the classical molasses predictions of Subsection 2.E with $\Delta = -2\Gamma$ and $I/I_0 = 0.5$. The dashed curves are from similar calculations made using the damping coefficients of the polarization-gradient forces of Section 3. The upper dashed curve is from the polarization-rotation damping of Eq. (34), and the lower dashed curve is from the ellipticity-gradient damping of Eq. (35).

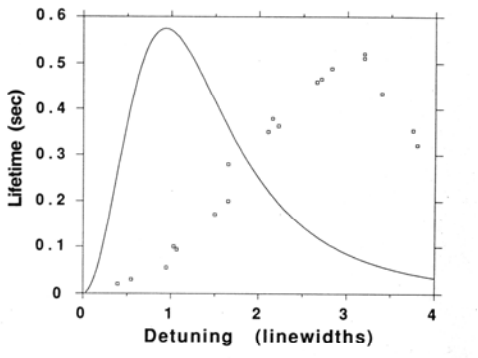

Fig. 9. Molasses lifetime versus laser detuning to the red of resonance. The open boxes are early experimental measurements made in our laboratory, while the solid curve is the prediction of Eq. (30) with $I/I_0 = 0.5$.

Molasses Experiment

temperature vs. turn off time

Lett et al. JOSA B6 p2084 (1989)

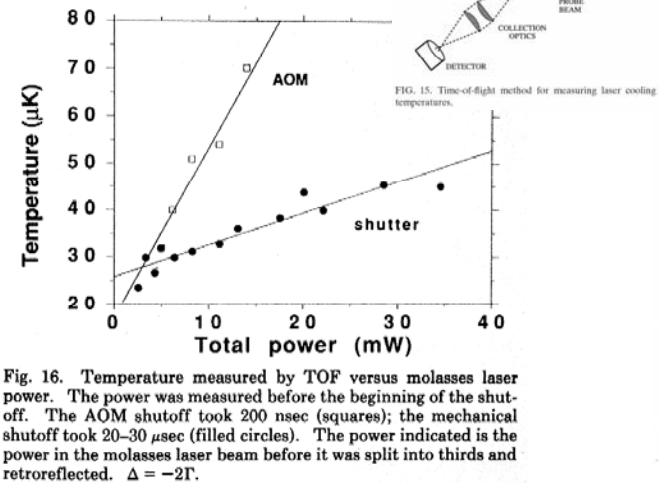

FIG. 15. Time-of-flight method for measuring laser cooling temperatures.

Fig. 16. Temperature measured by TOF versus molasses laser power. The power was measured before the beginning of the shut-off. The AOM shutoff took 200 nsec (squares); the mechanical shutoff took 20–30 μsec (filled circles). The power indicated is the power in the molasses laser beam before it was split into thirds and retroreflected. $\Delta = -2\Gamma$.

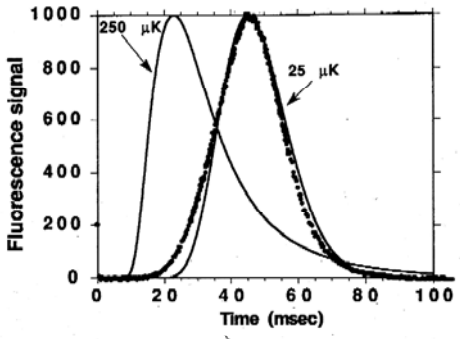

Fig. 11. TOF data and results of numerical calculations at 25 and 250 μK, all normalized to the same height. $\Delta = -2.5\Gamma$. The data points show fluorescence intensity versus time, and the solid curves indicate the expected signal.

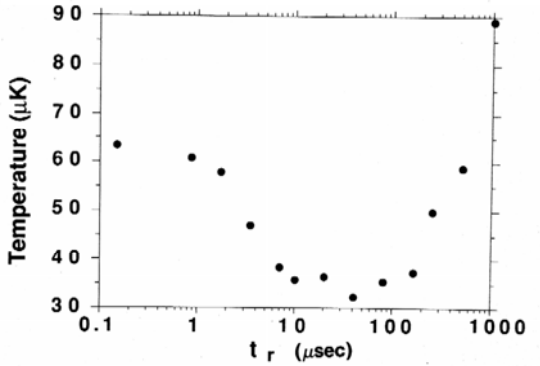

Fig. 15. Temperature measured by TOF as a function of turn-off time t_r. The quantity t_r is the time that it takes to ramp down the molasses laser beam intensity with an AOM.

Molasses Experiment

temperature

Lett et al. JOSA B6 p2084 (1989)

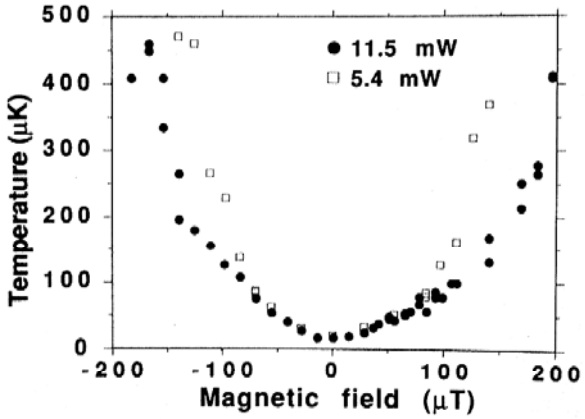

Fig. 19. Temperature versus magnetic field. The data were taken with a mechanical shutter. The two powers displayed were measured before the shutoff. $\Delta = -2\Gamma$.

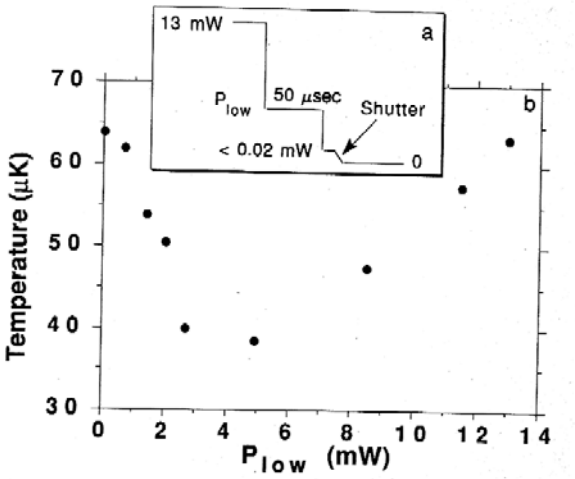

Fig. 17. a, Molasses laser power as a function of time for the data in b. The mechanical shutter shuts off approximately 10 μsec after the AOM. b, Temperature versus P_{LOW} showing that low-power molasses beams cool the atoms despite a fast shut-off. $\Delta = -2\Gamma$.

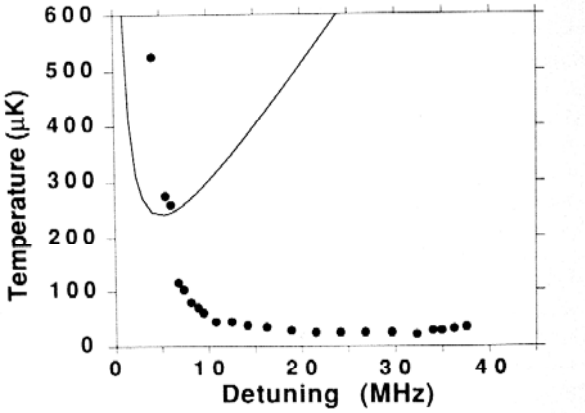

Fig. 20. Measured temperature versus laser detuning Δ, to the red of resonance. Also shown is the prediction of classical, low-power, one-dimensional molasses (solid curve), Eq. (12).

Light Forces in Multilevel Atoms

light shift, Sisyphus Effect

J. Dalibard, C. Cohen-Tannoudji JOSA B6 p2023 (1989)

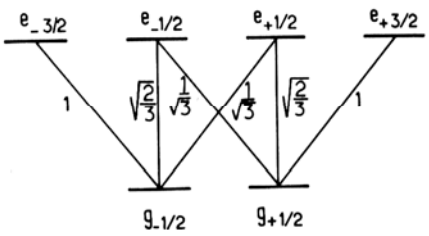

Fig. 2. Atomic level scheme and Clebsh–Gordan coefficients for a $J_g = 1/2 \leftrightarrow J_e = 3/2$ transition.

Atoms in light field: Dresses States

coupplied 2-state system Atom <-> Light

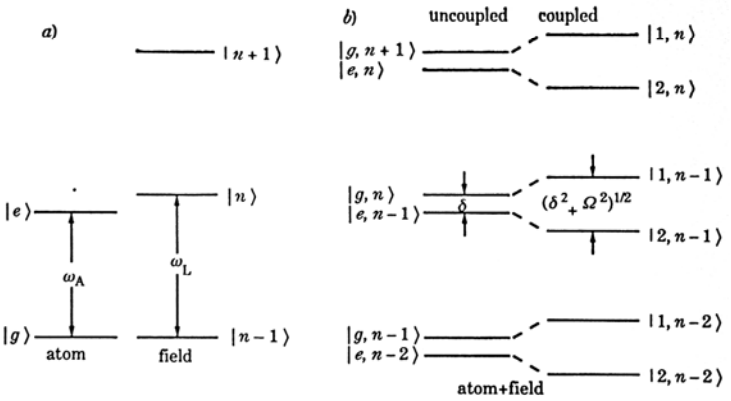

Fig. 19. – a) Energy levels of the atom and the field in the bare basis. b) Dressed basis of atom + field, with the atom uncoupled and coupled to the field.

$U = \frac{\hbar\Omega^2}{\delta}$	potential
$\rho_{ee} = \frac{\Omega^2}{\delta^2}$	excited state population
$R = \frac{\Omega^2}{\delta^2}\Gamma$	scattering rate

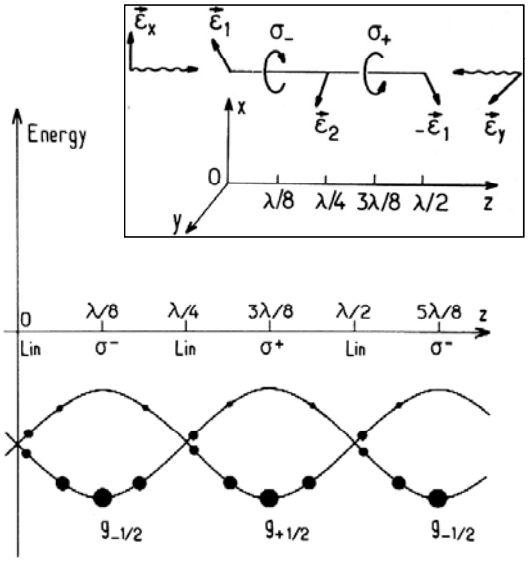

Fig. 3. Light-shifted energies and steady-state populations (represented by filled circles) for a $J_g = 1/2$ ground state in the lin ⊥ lin configuration and for negative detuning. The lowest sublevel, having the largest negative light shift, is also the most populated one.

Cooling Limit for Sisyphus Effect

J. Dalibard, C. Cohen-Tannoudji JOSA B6 p2023 (1989)

Estimation of the cooling force

$$\langle F_{pg} \rangle \approx U_0 \left(\frac{v\tau_p}{\lambda}\right)\frac{1}{\lambda} \approx \frac{\hbar\Omega^2}{\delta} k^2 v \frac{\delta^2}{\Omega^2\Gamma} = \hbar k^2 \frac{\delta}{\Gamma} v$$

full calc: $\alpha_{pg} = 3\hbar k^2 \frac{\delta}{\Gamma}$

compare to Doppler cooling: $\alpha_{dop} = \frac{\hbar k^2}{4}$

estimate the cooling limit:
Sisyphus heating:
force fluctuates as the atoms pump between the two levels:

$$2D_{pg} = \langle \dot{p}^2 \rangle$$

$$\approx \left(\frac{\hbar\Omega^2}{|\delta|}k\right)^2 \frac{1}{\tau_p} \approx \frac{\hbar^2 k^2 \Omega^2}{\Gamma}$$

cooling limit: $k_B T = \frac{D_{pg}}{\alpha} \approx \frac{\hbar\Omega^2}{\delta}$

full calcualtion for $|\delta| << \Gamma$: $k_B T = \frac{\hbar\Omega^2}{8|\delta|}$

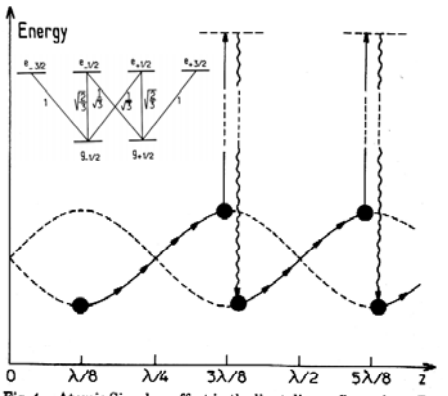

Fig. 4. Atomic Sisyphus effect in the lin ⊥ lin configuration. Because of the time lag τ_p due to optical pumping, the atom sees on the average more uphill parts than downhill ones. The velocity of the atom represented here is such that $v\tau_p \sim \lambda$, in which case the atom travels overs λ in a relaxation time τ_p. The cooling force is then close to its maximal value.

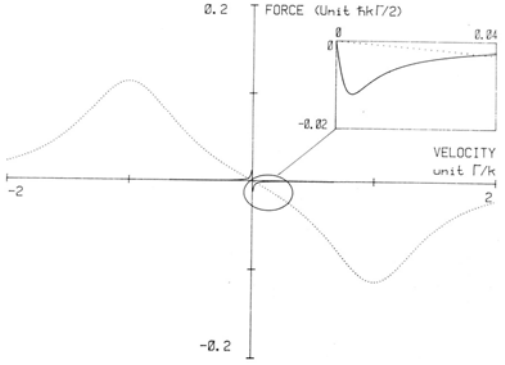

Fig. 7. Variations with velocity v of the force due to polarization gradients in the lin ⊥ lin configuration for a $J_g = 1/2 \leftrightarrow J_e = 3/2$ transition (solid curve). The values of the parameters are $\Omega = 0.3\Gamma$, $\delta = -\Gamma$. The dotted curve shows sum of the two radiation pressure forces exerted independently by the two Doppler-shifted counterpropagating waves. The force due to polarization gradients leads to a much higher friction coefficient (slope at $v = 0$) but acts on a much narrower velocity range.

$\sigma^+ - \sigma^-$ Molasses

J. Dalibard, C. Cohen-Tannoudji JOSA B6 p2023 (1989)

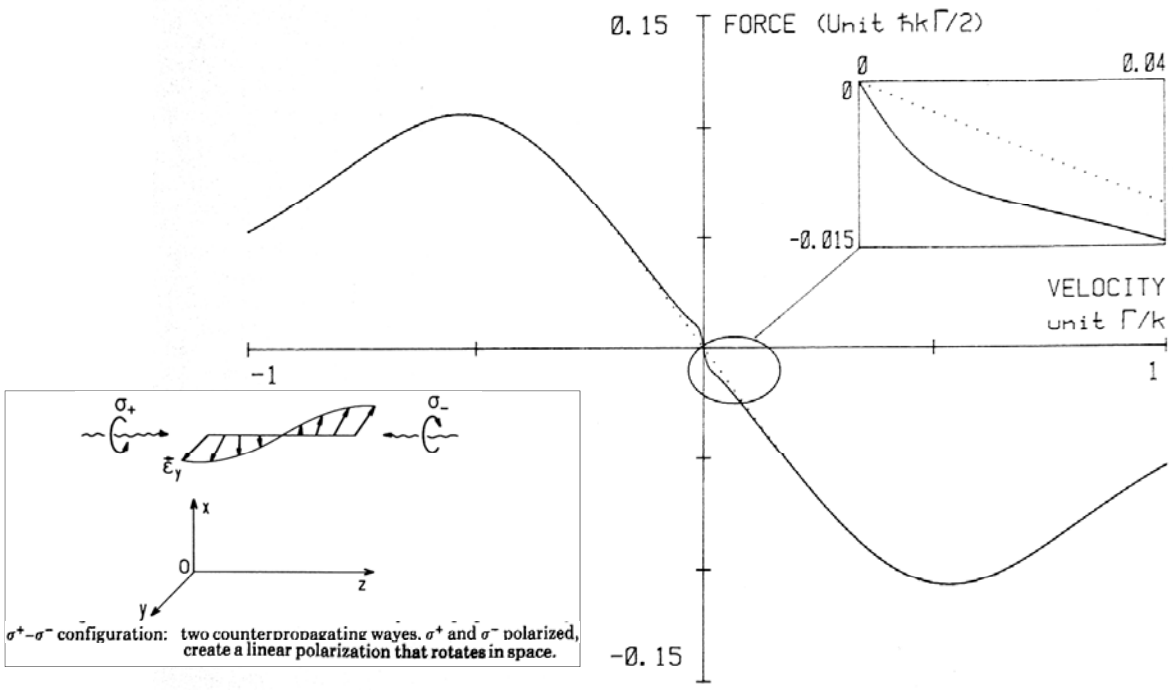

Fig. 8. Variations with velocity of the steady-state radiative force for a $J_g = 1 \leftrightarrow J_e = 2$ transition in the $\sigma_+ - \sigma_-$ configuration ($\Omega = 0.25\ \Gamma$; $\delta = -0.5\ \Gamma$). The slope of the force near $v = 0$ is very high (see also inset), showing that there is polarization gradient cooling. This new cooling force acts in the velocity range $kv \sim \Delta'$. Outside this range, the force is nearly equal to the Doppler force (shown by the dotted curve) calculated by neglecting all coherences between ground-state sublevels $|g_m\rangle_z$.

Molasses Experiment

Polarisation Gradient Cooling

C. Salomon et al. EPL **12** p683 (1990)

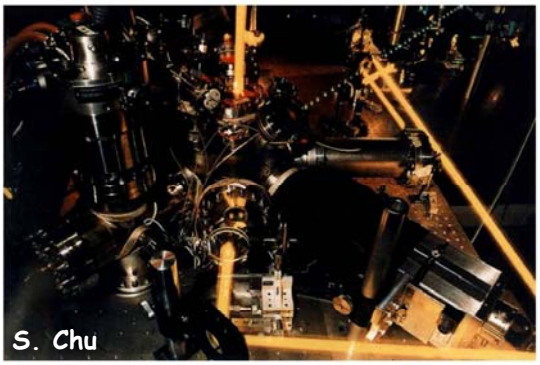

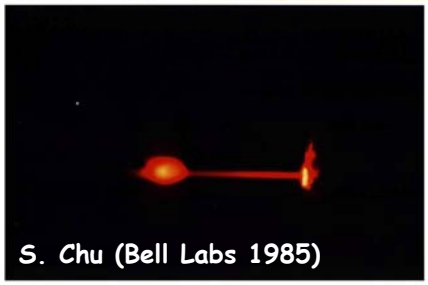

FIG. 4. (Color) A photograph of sodium atoms confined in our optical molasses experiment. The atoms were precooled by a counterpropagating laser before entering the region of six crossed laser beams.

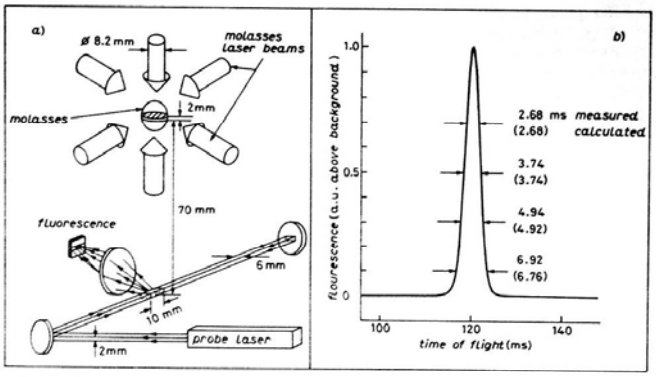

Fig. 1. – *a*) Apparatus: atoms from a laser-cooled atomic beam (not shown) are further cooled and confined at the intersection of three pairs of mutually orthogonal, counterpropagating laser beams. Cold atoms from a 2 mm high slice of the molasses are dropped into the probe. The probe-induced fluorescence is collected by a lens, imaged onto a photodiode, and recorded *vs.* time. *b*) Experimental time-of-flight spectrum for the lin⊥lin configuration with $|\delta|/2\pi = 52$ MHz and $\Omega^2/\Gamma^2 = 0.22$, $T = 2.5\ \mu$K. By comparing the measured widths of the TOF spectrum at various fractions of its full height with the calculated ones, we confirm that the initial velocity distribution is closely Maxwellian and can be assigned a temperature.

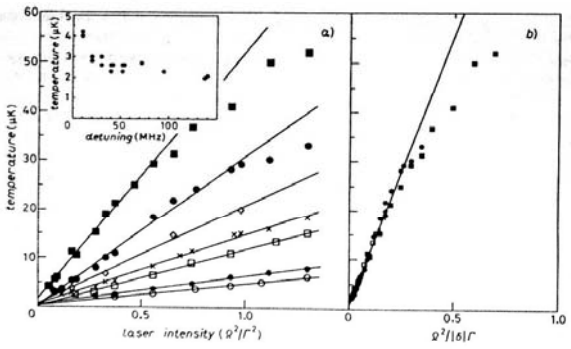

Fig. 2. – Temperature as a function of laser intensity and detuning. *a*) The lines are least-squares fits to those points which for a given detuning are within the range of validity of eq. (1). Insert: lowest temperature achieved as a function of detuning, for both polarization configurations. For $|\delta| \gg \Gamma$ ($\Gamma/2\pi = 5.3$ MHz) the lowest temperature is essentially constant. *b*) Temperatures of *a*) plotted against $\Omega^2/|\delta|\Gamma$. The straight line is a fit to the points with small $\Omega^2/|\delta|\Gamma$. $|\delta|/2\pi = 10$ MHz (■), 20 MHz (●), 30 MHz (◇), 40 MHz (×), 54 MHz (□), 95 MHz (•), 140 MHz (○).

Light Pressure Traping

1D and 2D lenses

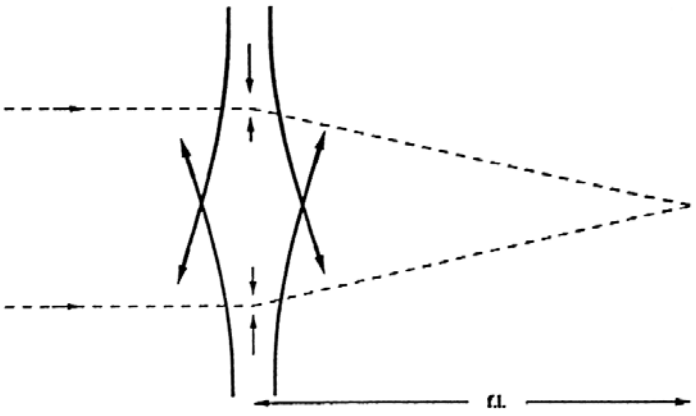

Fig. 14. – Radiation pressure 1-D lens.

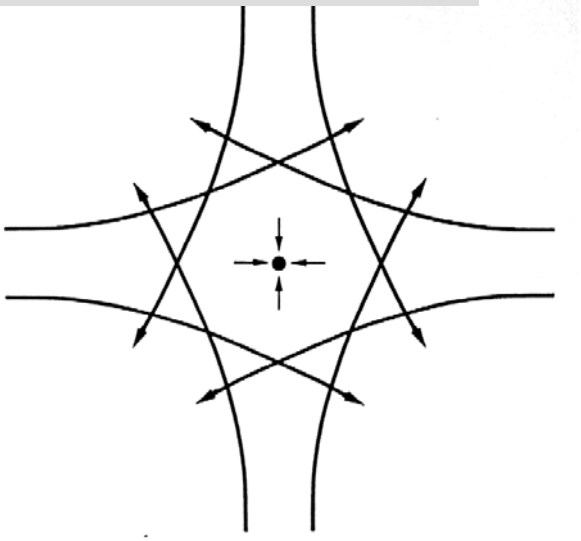

Fig. 15. – Radiation pressure trap in 2-D, formed by four focussed beams of circular cross-section.

- **Optical Earnshaw's theorem:**
  If the light scattering force is proportional to the local Pointing vector, it is impossible to construct an optical trap.

Magneto Optic Trap

E. Raab et al. PRL **59** p2631 (1987)

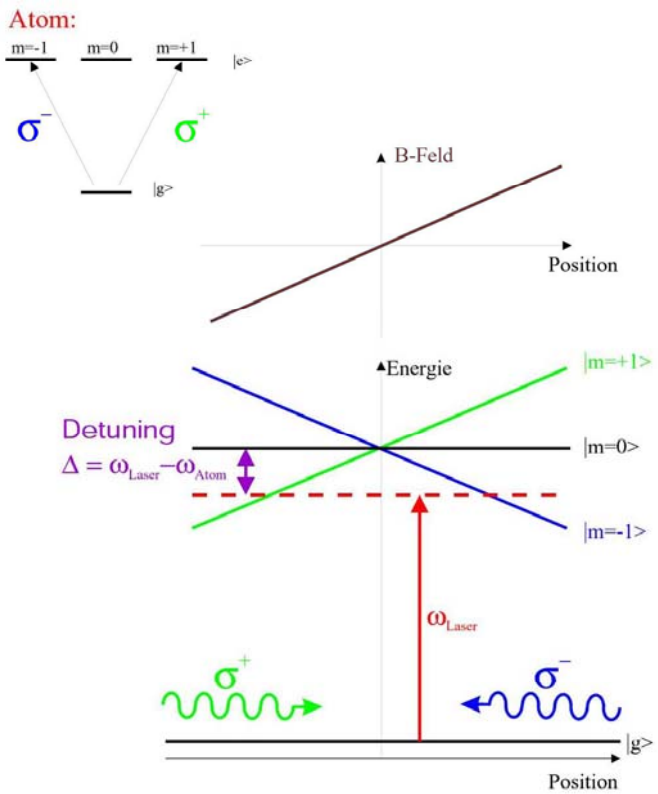

3d magnetic field realization:
Quadrupole

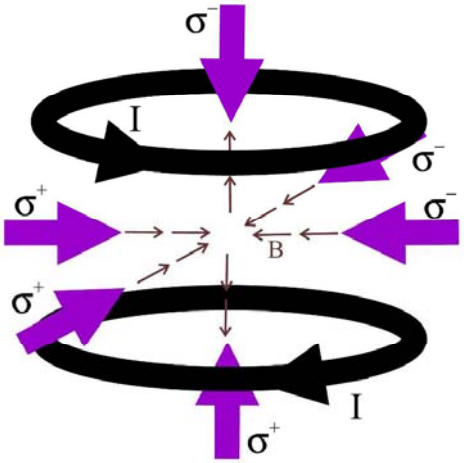

Atoms are pushed to the point with B=0

Typical parameters:

Density:	$>10^{11}$ atoms/cm^3
Up to	$>10^{10}$ atoms

Velocity Selective Coherent Population Trapping

R. Kaiser et al.
PRL **61** p826
(1988)

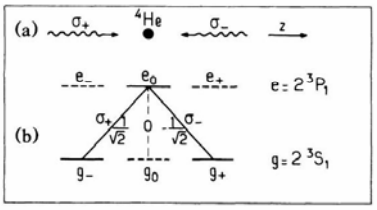

FIG. 1. (a) Two counterpropagating σ_+ and σ_- polarized laser beams interact with ^{4}He atoms on the 2^3S_1-2^3P_1 transition. (b) The Zeeman sublevels, and some useful Clebsch-Gordan coefficients. Since the $e_0 \leftrightarrow g_0$ transition is forbidden, all atoms are pumped into g_+ and g_- after a few fluorescence cycles. These two levels are coupled only to e_0, and a closed three-level Λ configuration is realized (solid lines).

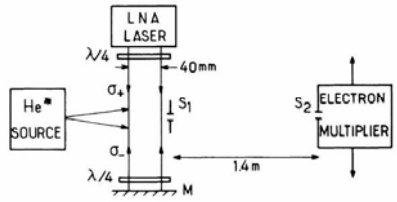

FIG. 3. Schematic experimental setup. The atomic source at 77 K produces a beam of metastable triple helium atoms (2^3S_1) at an average velocity of 1100 m/s. These atoms interact with two σ_+ and σ_- polarized counterpropagating waves at 1.08 μm. The transverse velocity distribution at the end of the interaction region is analyzed with two slits S_1 and S_2, 100 μm wide. S_2 is the entrance slit of a movable He* detector.

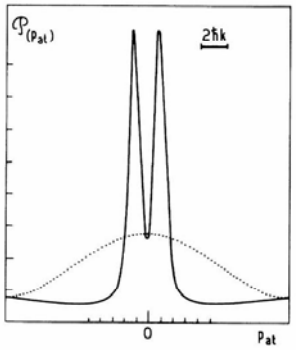

FIG. 2. Calculated transverse atomic momentum distribution resulting from cooling by velocity-selective coherent population trapping, for parameters close to our experimental situation (zero detuning, Rabi frequency $\omega_1 = 0.6\Gamma$, interaction time $\Theta = 350\Gamma^{-1}$). The initial distribution is represented by a dotted line.

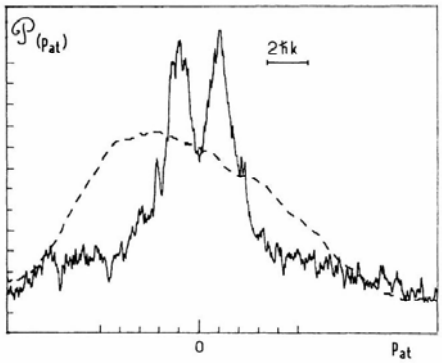

FIG. 4. Transverse atomic momentum profile at the end of the interaction region, with the laser on (solid line) and off (dashed line; this profile has been smoothed). The double-peak structure at about $\pm \hbar k$ and above the initial distribution is a clear signature of the cooling effect presented in this Letter.

Coupled Pendulum Model

P.Hemmer, M. Prentiss J. Opt. Soc. Am. B **5**, 1613 (1988)

Table 1. Summary of Correspondences between the Stimulated Resonance Raman Interaction (Three-Level Atom) and a Set of Three Classical Coupled Pendulums[a]

Coupled-Pendulum System	Three-Level Atom
Pendulum oscillations η_1, η_2, η_3	Atom–field composite states $\|1\rangle\|\omega_1\rangle, \|2\rangle, \|3\rangle\|\omega_2\rangle$
Coupling springs $\Omega_1' = \frac{k_1}{M\omega_1'}, \Omega_2' = \frac{k_2}{M\omega_2'}$	Laser-field coupling $\Omega_1 = \frac{\mu_{21}E_1}{\hbar}, \Omega_2 = \frac{\mu_{23}E_2}{\hbar}$
Frictional damping γ_2'	Spontaneous emission γ_2
Pendulum oscillation amplitudes N_1, N_2, N_3	Composite-state amplitudes A_1, A_2, A_3
Pendulum energy ($+\frac{1}{2}M\omega_k'^2$) $\|N_1\|^2, \|N_2\|^2, \|N_3\|^2$	Composite-state probability $\|A_1\|^2, \|A_2\|^2, \|A_3\|^2$
Pendulum natural frequency $\omega_1', \omega_2', \omega_3'$	Composite-state energy ($\div\hbar$) $\frac{\epsilon_1}{\hbar}, \frac{\epsilon_2}{\hbar}, \frac{\epsilon_3}{\hbar}$
Normal modes $n_-, (n_+, \eta_2)$	Dressed states $\|-\rangle, \|+\rangle$

[a] Relevant notations are also introduced.

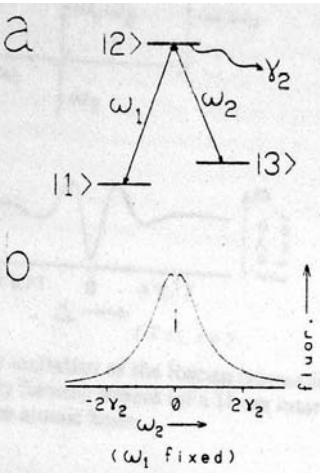

Fig. 1. a, Schematic diagram of stimulated resonance Raman interaction. b, Experimental data showing the Raman interaction as a decrease in fluorescence.

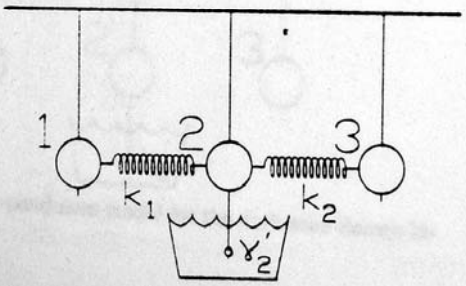

Fig. 2. Coupled-pendulum model for the stimulated resonance Raman interaction.

Coupled Pendulum Model

P.Hemmer, M. Prentiss
J. Opt. Soc. Am. B **5**, 1613 (1988)

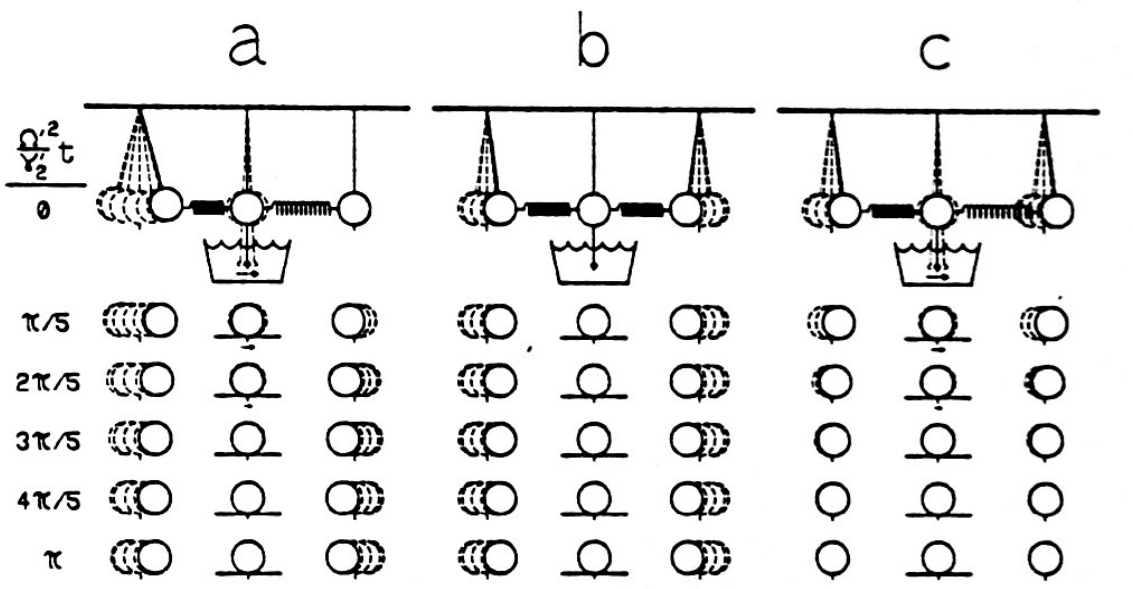

a, Motion of the coupled-pendulum model in the case of equal coupling-spring strengths, $\Omega' = 0.2\gamma_2'$. b, Trapped-mode contribution to motion in a. c, Damped-mode contribution to motion in a.

Raman Cooling

M. Kasevich, S. Chu PRL **69** p1741 (1992)

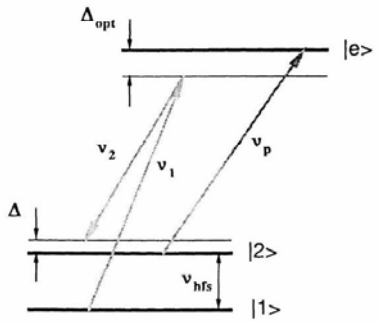

FIG. 1. Energy level diagram for Raman cooling.

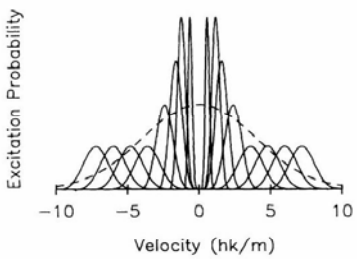

FIG. 2. The probability of excitation vs velocity for each of the sixteen sequentially applied stimulated Raman cooling pulses (solid lines) and the initial velocity distribution of atoms cooled in the polarization-gradient molasses (dashed line).

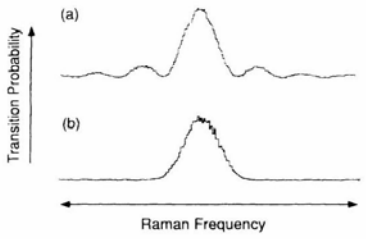

FIG. 3. Measured excitation probability vs frequency detuning for both (a) a square wave and (b) a Blackman pulse (defined as $\Omega(t) = \Omega_{\text{eff}}\{0.5\cos(\pi[2t/\tau - 1]) + 0.08\cos(2\pi[2t/\tau - 1]) + 0.42\}$ for $0 \le t \le \tau$).

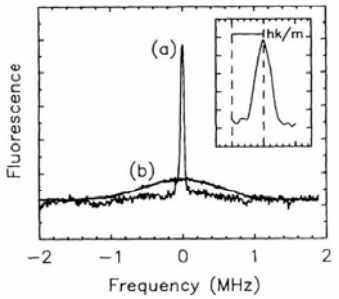

FIG. 4. (a) The velocity distribution after application of the stimulated Raman cooling pulses. The inset, showing a high resolution scan of the central velocity spike, compares the velocity distribution to the velocity change $\Delta v = 3$ cm/sec from the recoil of a single photon. (b) The initial velocity distribution of sodium atoms due to polarization-gradient cooling. A uniform background signal ~3 times the size of the peak signal for curve *b* has been subtracted from curve *a*. The background was due to incomplete optical pumping from $F = 2 \rightarrow F = 1$ during the Raman cooling sequence, and is responsible for the increased noise on curve *a*.

4.2 Mechanical effects of light II: The dipole force

Dressed state potentials
Dipole traps
- Optical Tweezers
- RF trap

Optical lattices

Atome im Lichtfeld

Dresses States

gekoppeltes 2-Zustandsystem Atom <-> Licht

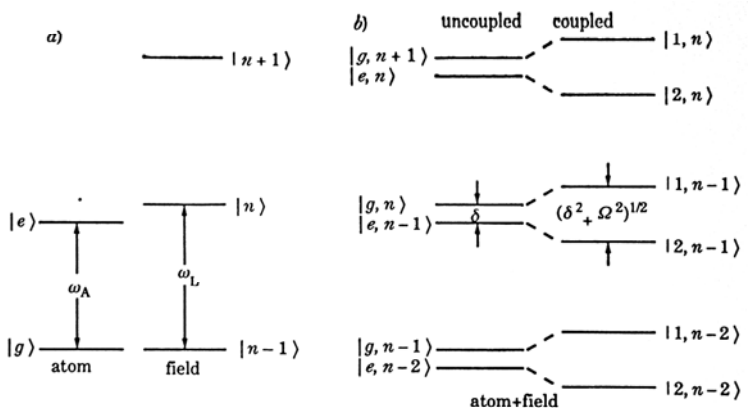

Fig. 19. – a) Energy levels of the atom and the field in the bare basis. b) Dressed basis of atom + field, with the atom uncoupled and coupled to the field.

$$U = \frac{\hbar\Omega^2}{\delta}$$ Potential

$$\rho_{ee} = \frac{\Omega^2}{\delta^2}$$ excited state population

$$R = \frac{\Omega^2}{\delta^2}\Gamma$$ scattering rate

Atoms in Gaussian laserbem

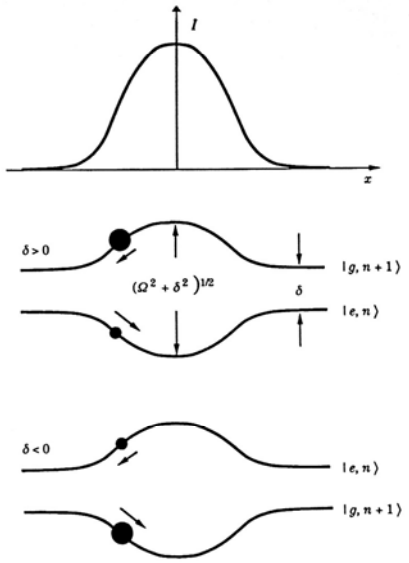

Dielectric Spheres

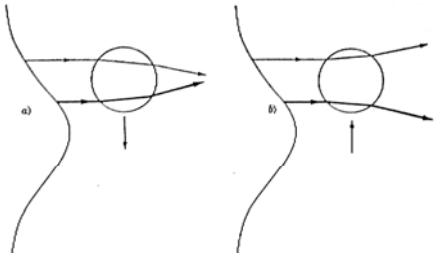

Optical Trapping

"Optical lattice" : 4 µm polystyrol particles on water surface
conservative light force for macroscopic particles → optical tweezers

2 beam lattice

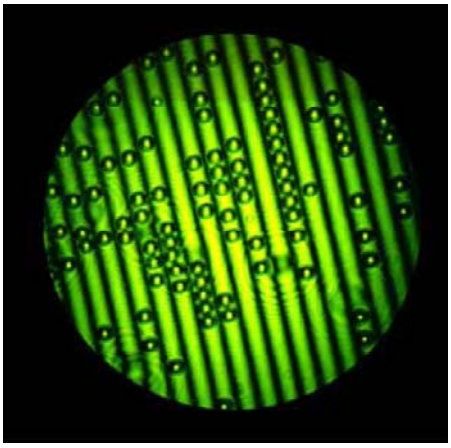

4 beam lattice

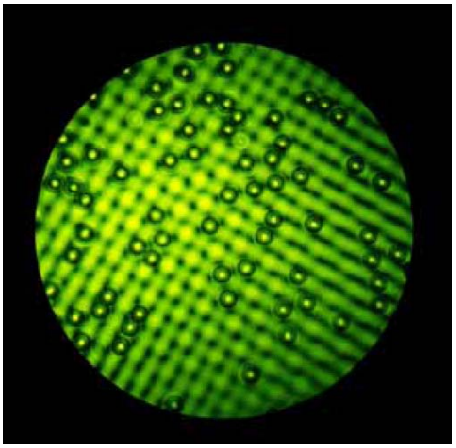

this is not (only) a joke: optical tweezers do amazing things in biology
(measure the force of a ribosome)

The dipole force

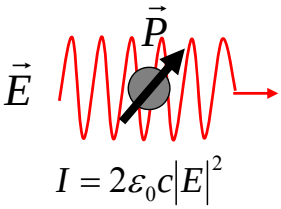

Induced electric polarization of an atom in a laser field:

$$\vec{p} = \alpha \vec{E}$$

the resulting **interaction potential** is $V_{dip} = -\frac{1}{2}\left\langle \vec{p}\vec{E} \right\rangle = -\frac{1}{2\varepsilon_0 c}\mathrm{Re}(\alpha) I$ („in phase")

and the **scattering rate** $\Gamma_{scat} = \frac{P_{abs}}{\hbar\omega} = \frac{1}{\hbar\varepsilon_0 c}\mathrm{Im}(\alpha) I$ („out of phase")

$V_{dip} \propto I/\delta$
$\Gamma_{scat} \propto I/\delta^2$

} go for high detuning and high intensity

red detuned laser

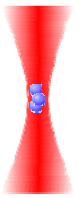

($\delta < 0$)

blue detuned laser

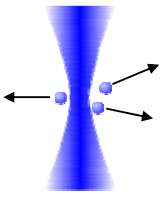

($\delta > 0$)

In most optical lattices lasers are blue detuned to avoid photon scattering

Atom – Light Interaction

open 2-level system:

complex optical potential:

$$V_{Opt} = \hbar \frac{\Omega_{Rabi}^2}{4\Delta + i2\Gamma}$$

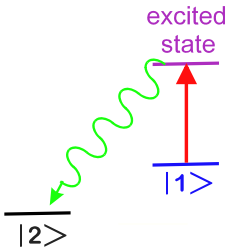

with: coupling $\hbar\Omega_{Rabi} = d_e E$

laser detuning $\Delta = \omega_{Laser} - \omega_{Atom}$

decay rate Γ

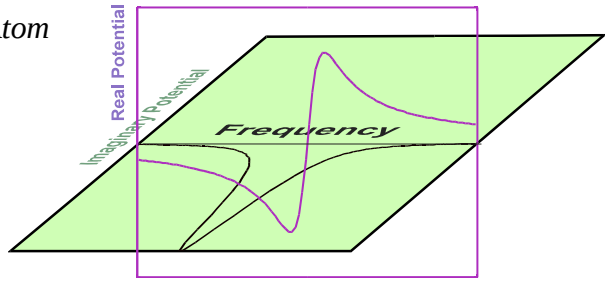

Real part: refraction, phase shift
Imaginary part: absorption
(if state |2> is not detected)

Optical Lattices

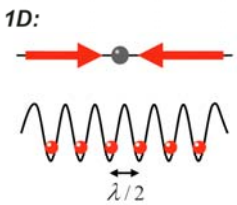

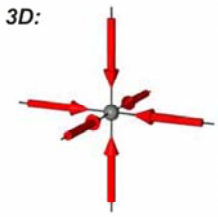

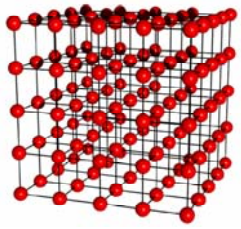

$$V(\vec{r}) \propto \sin^2(kx) + \sin^2(ky) + \sin^2(ky) \quad + \textit{weak harmonic confinement}$$

- the resulting potential is a simple cubic lattice
- the lattice potential is perfect: no defects, no slips
- the BEC coherently spreads over more than 100.000 lattice sites
- filling per site: 1-3 atoms
- potential depth can be adjusted between 0..50 E_{recoil}
- typical trap frequency per site ≈ 2π x 50 kHz

$$E_{recoil} = \frac{\hbar^2 k^2}{2m}$$

Standing Light Wave

Interference of two light waves $\vec{k}_1$ $\vec{k}_2$

$$E^2(\vec{x}) = E_0{}^2\left[1+\cos\left((\vec{k}_1-\vec{k}_2)\vec{x}+\delta_0\right)\right]$$
$$= E_0{}^2\left[1+\cos\left(\vec{G}\vec{x}+\delta_0\right)\right]$$

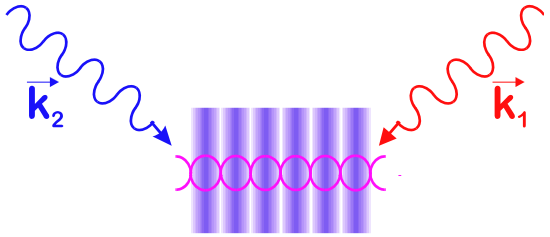

Consider retro reflection of light from a mirror ($\vec{k}_1 = -\vec{k}_2$)
and therefore a grating vector $\vec{G} = \vec{k}_1 - \vec{k}_2 = 2\vec{k}$

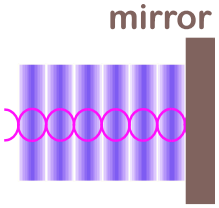

Far off resonant light: phase grating

$$U(x) = \frac{\hbar\Omega_0{}^2}{4\Delta}\left(1+\cos(\vec{G}\vec{x}+\delta_0)\right)$$

On resonant light: absorption grating

$$U(x) = i\frac{\hbar\Omega_0{}^2}{2\Gamma}\left(1+\cos(\vec{G}\vec{x}+\delta_0)\right)$$

transmission (thin grating):

$$T(x) \cong \exp\left(-A_0\left(1+\cos(\vec{G}\vec{x}+\delta_0)\right)\right)$$

Diffraction on a Standing Light Wave

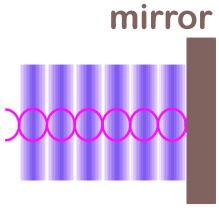

Large Laser Detuning: $\Delta >> \Gamma$

$$U(x) = \frac{\hbar\Omega_0{}^2}{4\Delta}\left(1+\cos(\vec{G}\vec{x}+\delta_0)\right)$$

Beugung am dünnen Gitter

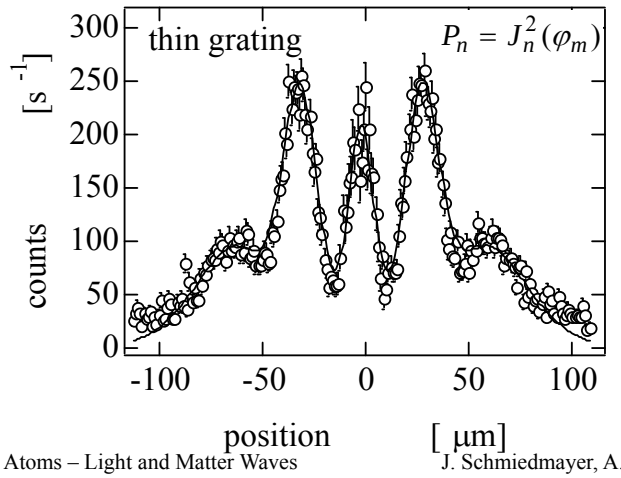

Bragg diffraction

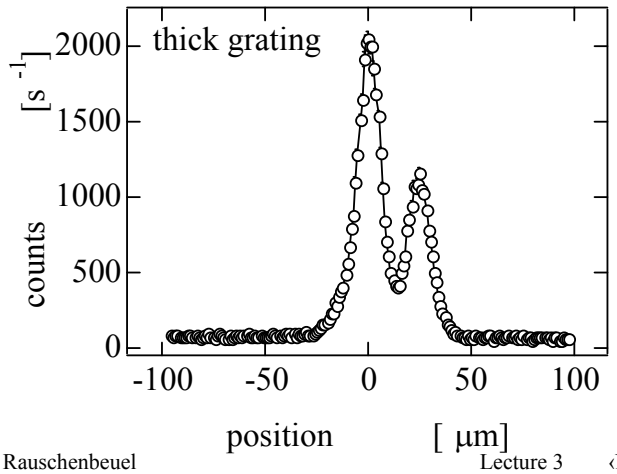

Diffraction from a standing light wave

Recoil picture: photon scattering

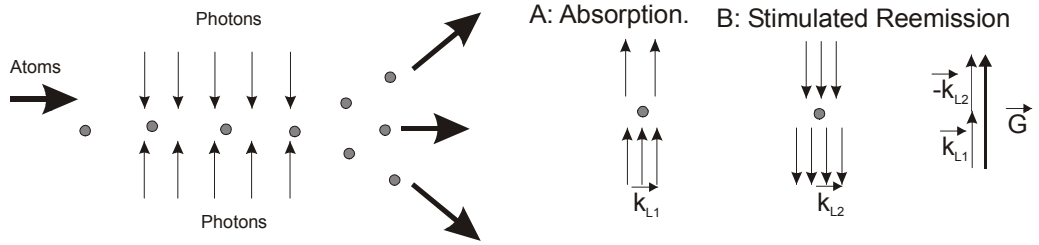

Atom gets 2 photon recoils $\pm 2\hbar k_L$

Wave picture: diffraction

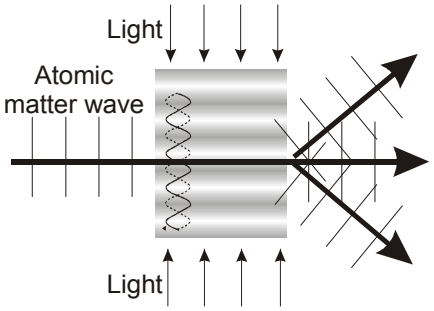

Light-grating vector: $G = 2k_L$

$\Rightarrow$ **Atomic momentum change: $\pm 2\hbar k_L$**

Light as a refractive index grating:

Thin and Thick Gratings

Thick grating the k-vectors of the light are very well defined and momentum transfer can only be in specific directions -> Bragg condition

Thin grating has many different k-vectors
allows stimulated scattering for a variety of incident angles

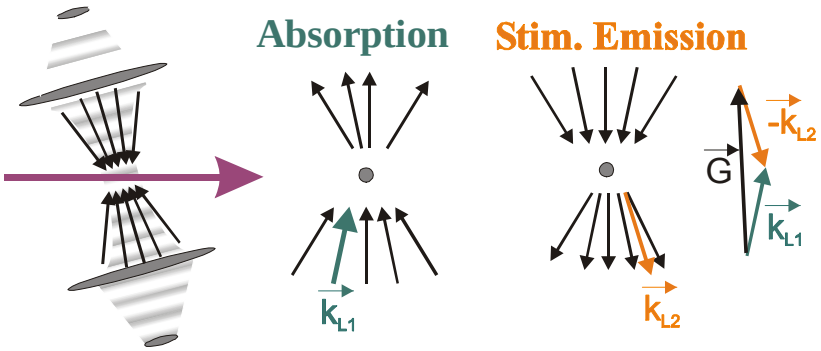

How many grating planes are crossed?

light crystal
$L > L_{Talbot}$

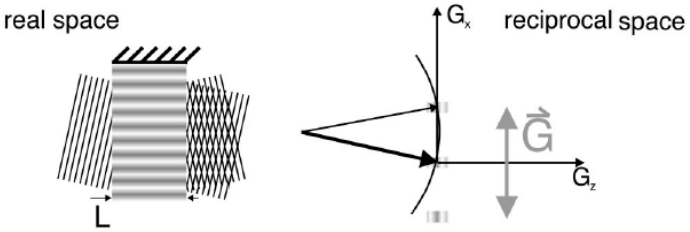

light grating
$L < L_{Talbot}$

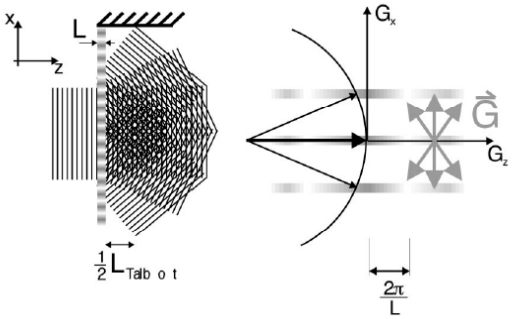

4.3 Controlling Atoms with Light
Controlling Light with Atoms

Coherent population transfer
STImulated Raman Adiabatic Passage (STIRAP)
Electromagnetically Induced Transparency (EIT)
Slow Light,
Stopping Light

Coherent Population Transfer I

K. Bergmann et al. Rev. Mod. Phys. **70**, 1003 (1998).

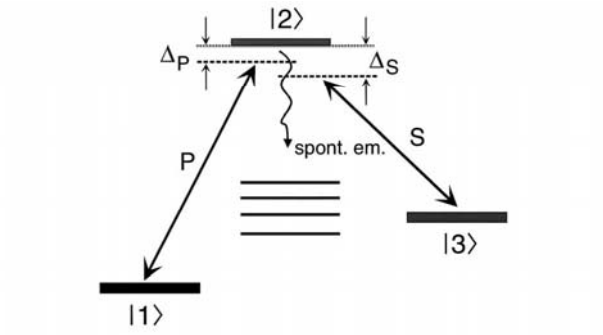

FIG. 1. Three-level excitation scheme. The initially populated state $|1\rangle$ and the final state $|3\rangle$ are coupled by the Stokes laser S and the pump laser P via an intermediate state $|2\rangle$. This latter state may decay by spontaneous emission to other levels. The detuning of the pump and Stokes laser frequencies from the transition frequency to the intermediate state are Δ_P and Δ_S, respectively.

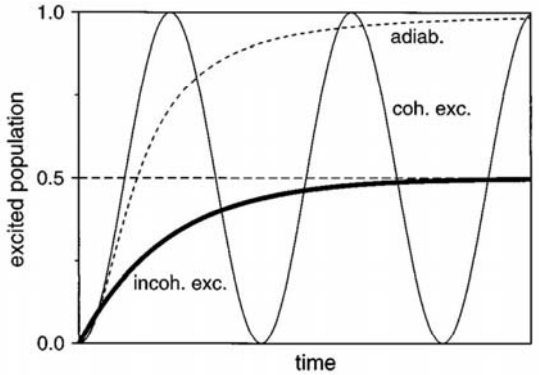

FIG. 2. Evolution of the population of the upper level in a two-level system, driven by a coherent radiation field (thin line), by an incoherent radiation field (heavy line), and by an adiabatic passage process (dashed line).

Coherent Population Transfer III

K. Bergmann et al. Rev. Mod. Phys. **70**, 1003 (1998).

coupled 3 state system (non degenerate):

$$H(t)=\frac{\hbar}{2}\begin{bmatrix} 0 & \Omega_P(t) & 0 \\ \Omega_P(t) & 2\Delta_P & \Omega_S(t) \\ 0 & \Omega_S(t) & 2(\Delta_P-\Delta_S) \end{bmatrix}.$$

dressed state eigenen staets

$$|a^+\rangle=\sin\Theta\sin\Phi|1\rangle+\cos\Phi|2\rangle+\cos\Theta\sin\Phi|3\rangle,$$

$$|a^0\rangle=\cos\Theta|1\rangle-\sin\Theta|3\rangle,$$

$$|a^-\rangle=\sin\Theta\cos\Phi|1\rangle-\sin\Phi|2\rangle+\cos\Theta\cos\Phi|3\rangle, \quad (8)$$

where the (time-varying) mixing angle Θ is defined by the relationship

$$\tan\Theta=\frac{\Omega_P(t)}{\Omega_S(t)}. \quad (9)$$

dressed state eigenen energies

$$\omega^+=\Delta_P+\sqrt{\Delta_P^2+\Omega_P^2+\Omega_S^2}, \quad \omega^0=0,$$

$$\omega^-=\Delta_P-\sqrt{\Delta_P^2+\Omega_P^2+\Omega_S^2}.$$

adiabaticity condition

$$\left|\frac{\dot\Omega_P\Omega_S-\Omega_P\dot\Omega_S}{\Omega_P^2+\Omega_S^2}\right|\ll|\omega^\pm-\omega^0|,$$

$\Omega_{eff}\Delta\tau>10$, with $\Omega_{eff}=\sqrt{\Omega_P^2+\Omega_S^2}$

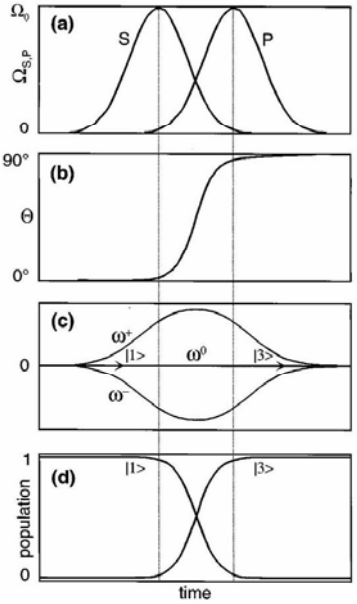

FIG. 3. Time evolution of (a) the Rabi frequencies of the pump and Stokes laser (see Fig. 1); (b) the mixing angle [see Eq. (9)]; (c) the dressed-state eigenvalues [see Eq. (10)]; and (d) the population of the initial level (starting at unity) and the final level (reaching unity).

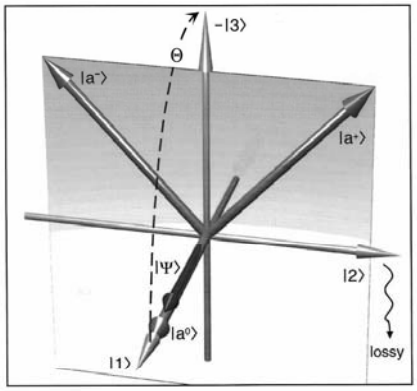

FIG. 4. Graphic representation of the Hilbert space for the three-level system in the basis of the bare states ($|1\rangle$, $|2\rangle$, and $|3\rangle$) and in the basis of the dressed states $|a^0\rangle$, $|a^+\rangle$, and $|a^-\rangle$. When the Stokes laser is much stronger than the pump laser (phase I, see Fig. 3), the state vectors $|1\rangle$ and $|a^0\rangle$ are aligned parallel to each other. Since the population is initially in state $|1\rangle$, the state vector is also aligned parallel to $|1\rangle$. At later times, the components of the state vector along the three dressed or bare states give the population in these states.

Coherent Population Transfer II

K. Bergmann et al. Rev. Mod. Phys. **70**, 1003 (1998).

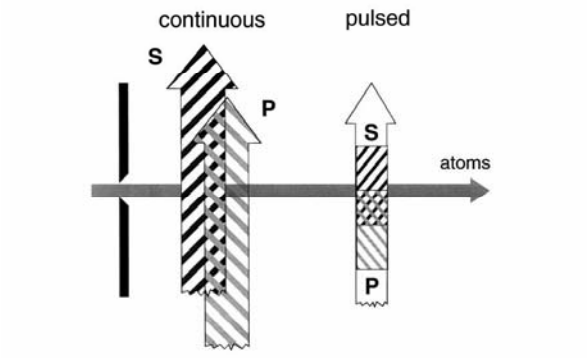

FIG. 5. Schematics of the STIRAP setup for population transfer for particles in a molecular beam. When continuous laser radiation is used, the STIRAP sequences (Stokes before pump) is implemented by spatially shifting the axes of the S and P lasers relative to each other. When pulsed lasers are used, the STIRAP sequence is implemented by appropriate time delay of the pulses.

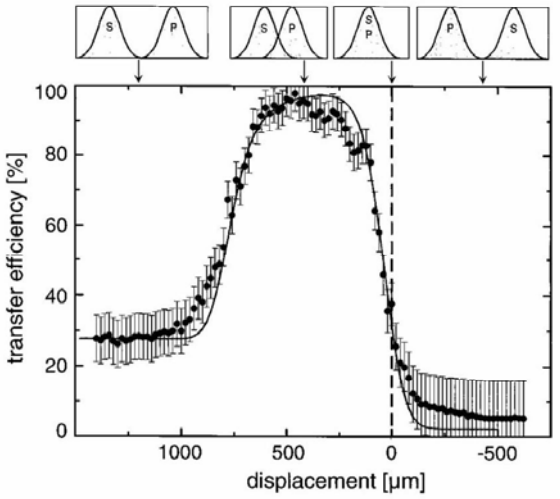

FIG. 9. Population transfer from the $^3P_0$ state to the $^3P_2$ state (see Fig. 6), induced by a continuous laser, as a function of the overlap between the Stokes and the pump lasers (shown on top).

Electromagnetically Induced Transparency I

general Λ -system
- two atomic ground states
- one common excited state

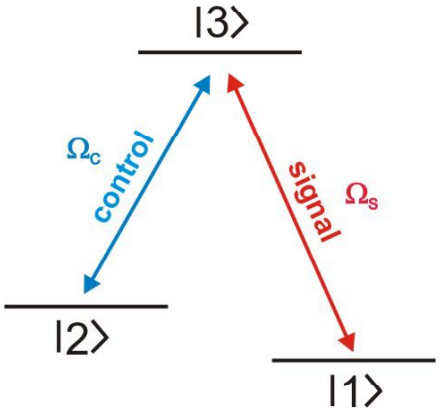

Λ-system Hamiltonian (RWA) in presence of two light fields

$$H(t) = \frac{\hbar}{2}\begin{bmatrix} 0 & 0 & \Omega_s(t) \\ 0 & 2(\Delta_s - \Delta_c) & \Omega_c(t) \\ \Omega_s(t) & \Omega_c(t) & 2\Delta_s \end{bmatrix}$$

Δ_s signal beam single photon det.

Δ_c control beam single photon det.

$\Omega_{s/c}$ Rabi Frequency of the signal/control field

Eigenstates at two-photon resonance (Δ_s- Δ_c=0)

$$\begin{aligned} |a^+\rangle &= \sin\Theta\sin\Phi|1\rangle + \cos\Theta\sin\Phi|2\rangle + \cos\Phi|3\rangle \\ |a^0\rangle &= \cos\Theta|1\rangle - \sin\Theta|2\rangle \\ |a^-\rangle &= \sin\Theta\cos\Phi|1\rangle + \cos\Theta\cos\Phi|2\rangle - \sin\Phi|3\rangle \end{aligned}$$

$$\tan\Theta = \frac{\Omega_s(t)}{\Omega_c(t)}$$

On two-photon-resonance state $|a^0\rangle$ has zero probability to be excited

$$\langle 3|\mu\cdot\varepsilon|a^0\rangle = 0 \quad \Leftrightarrow \quad \hbar\omega_s - \hbar\omega_c = E_2 - E_1$$

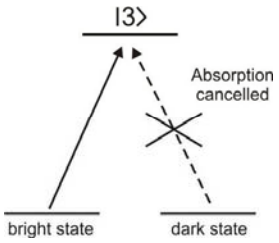

Electromagnetically Induced Transparency II
Dispersion in EIT Media

Control field off

Control field on

$\frac{dn}{d\omega_s}$ large but $\frac{d^2n}{d^2\omega_s} = 0$

Signal field absorption ~ Im(n)

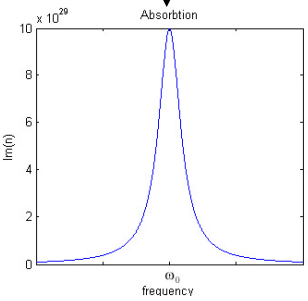

Signal field dispersion ~ Re(n)

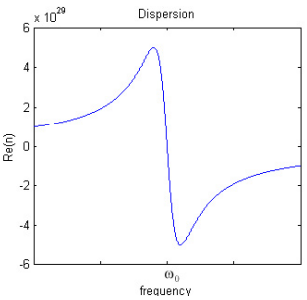

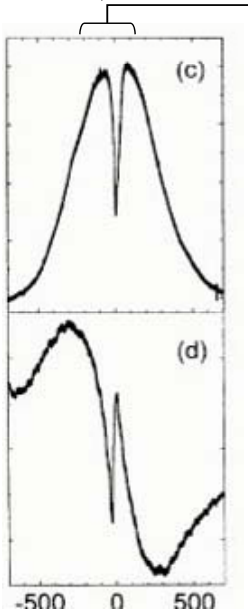

Xiao, PRL 74, 6663

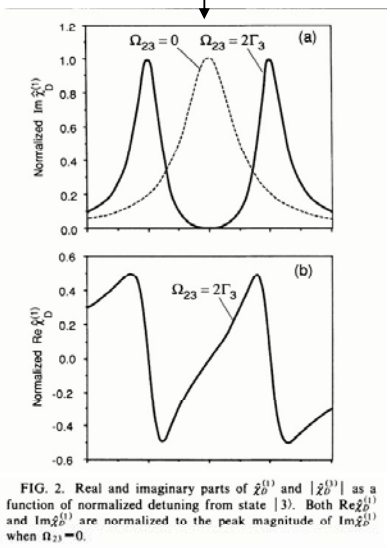

FIG. 2. Real and imaginary parts of $\tilde{\chi}_{ab}^{(1)}$ and $|\tilde{\chi}_{ab}^{(3)}|$ as a function of normalized detuning from state $|3\rangle$. Both $\mathrm{Re}\tilde{\chi}_{ab}^{(1)}$ and $\mathrm{Im}\tilde{\chi}_{ab}^{(1)}$ are normalized to the peak magnitude of $\mathrm{Im}\tilde{\chi}_{ab}^{(1)}$ when $\Omega_{23}=0$.

Harris, Physics Today, 1997

Electromagnetically Induced Transparency III
Slow Light, Stopping Light

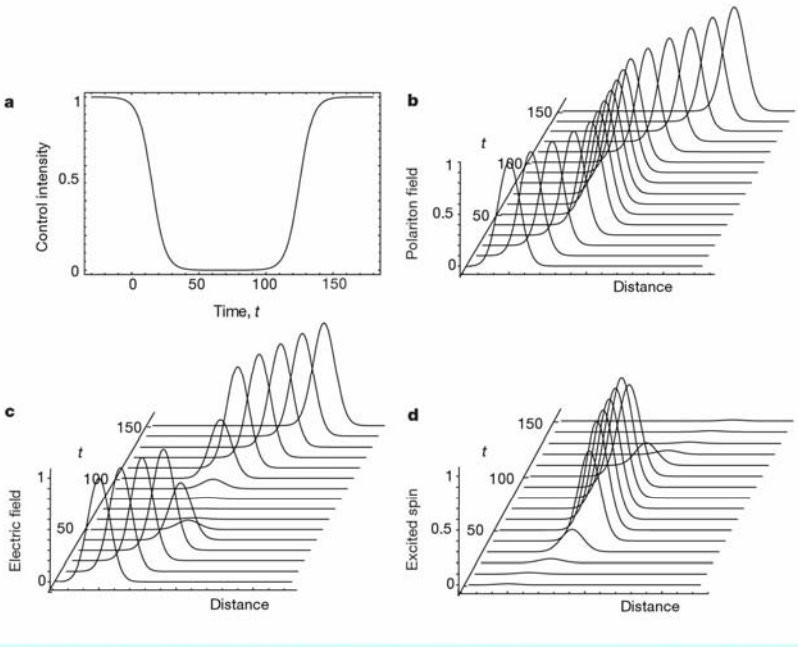

Figure 3 Dark-state polaritons. A dark-state polariton can be stopped and re-accelerated by ramping the control field intensity as shown in **a**. The coherent amplitudes of the polariton Ψ, the electric field E and the spin components S are plotted in **b** to **d**.

Electromagnetically Induced Transparency IV

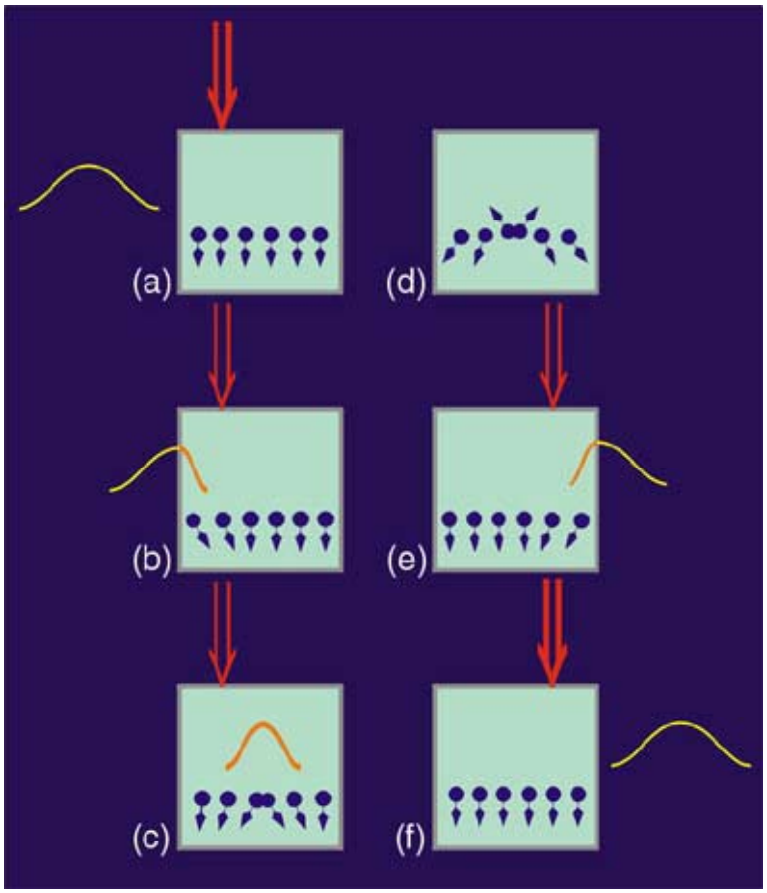

Light gets transferred into coherence between the ground state hyperfine levels. (a 2-state system)

Light is stored in this coherence

Readout: convert the coherence back into light.

Stored Light

Diplomarbeit D. Heine (HD-PI)

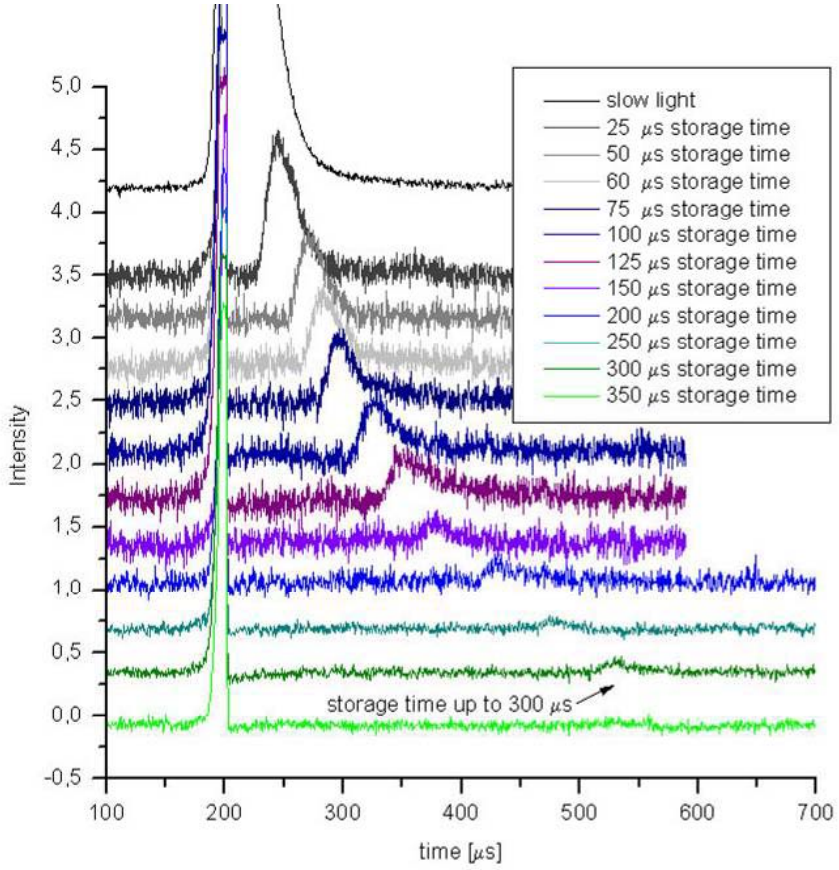

Storage of a 55 μs pulse for up to 300 μs

Electromagnetically Induced Transparency V

nonlinear optics

general Λ-system

- two atomic groundstates
- one common excited state

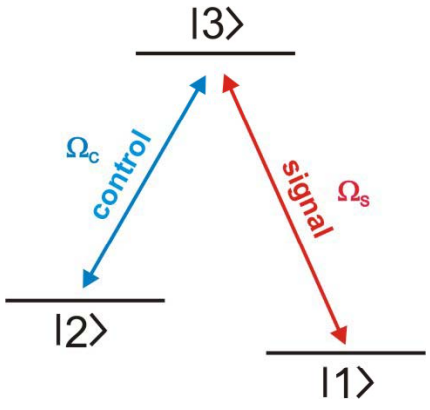

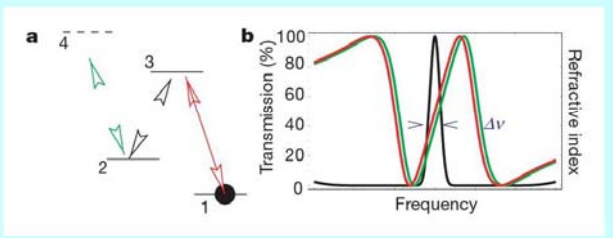

Figure 1 Electromagnetically induced transparency. **a**, Prototype atomic system for EIT and nonlinear optics. **b**, Spectrum of transmission and refractive index corresponding to EIT. Rapid variation of the refractive index (red curve) causes a reduction of group velocity. A control field (black arrow) is used to modify the propagation of weak resonant field (red) or to induce its interaction with another weak field (green). The presence of a second weak field causes an effective shift of the resonant frequency (green curve), which results in a corresponding change of the refractive index.

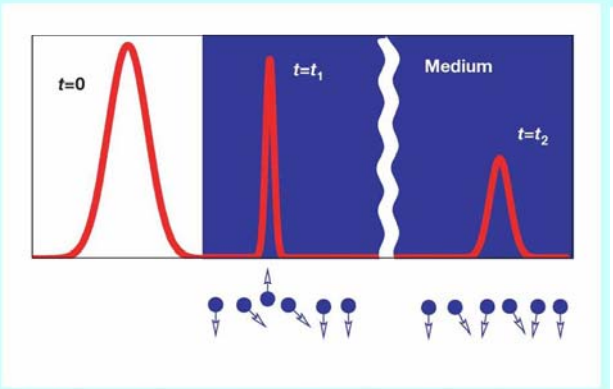

Figure 2 Schematic of spatial compression exhibited when a light pulse (red curve) enters the slow medium (blue). Photons are converted into flipped spins (blue arrowed circles), and the slow photonic and spin waves then propagate together. For long distances ($t_2 \gg t_1$), the lossless propagation is limited by the spreading of the pulses owing to the narrow bandwidth of the transparency window.

Stopping Light

D. F. Phillips et al. PRL **84**, 783 (2001);
Chien Liu et al. Nature **409**, 490 (2001).

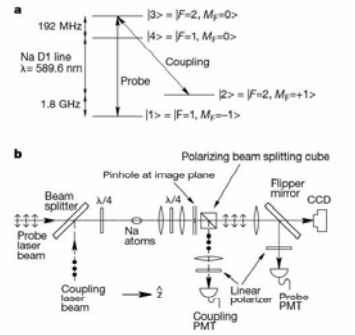

Figure 1 Experimental set-up and procedure. **a**, States |1⟩, |2⟩ and |3⟩ form the three-level EIT system. The cooled atoms are initially magnetically trapped in state $|1\rangle = |3S, F = 1, M_F = -1\rangle$. Stimulated photon exchanges between the probe and coupling laser fields create a 'dark' superposition of states |1⟩ and |2⟩, which renders the medium transparent for the resonant probe pulses. **b**, We apply a 2.2-mm diameter, σ^--polarized coupling laser, resonant with the $|3S, F = 2, M_F = +1\rangle \rightarrow |3P, F = 2, M_F = 0\rangle$ transition, and a co-propagating, 1.2-mm diameter σ^+-polarized probe pulse tuned to the $|3S, F = 1, M_F = -1\rangle \rightarrow |3P, F = 2, M_F = 0\rangle$ transition. The two laser beams start out with orthogonal linear polarizations (two-headed arrows and filled circles show the directions of linear polarization of the probe and coupling lasers, respectively). They are combined with a beam splitter, circularly polarized with a quarter-wave plate (λ/4), and then injected into the atom cloud. After leaving the cloud, the laser beams pass a second quarter-wave plate and regain their original linear polarizations before being separated with a polarizing beam-splitting cube. The atom cloud is imaged first onto an external image plane and then onto a CCD (charge-coupled device) camera. A pinhole is placed in the external image plane and positioned at the centre of the cloud image. With the pinhole and flipper mirror in place, only those portions of the probe and coupling laser beams that have passed through the central region of the cloud are selected and monitored simultaneously by two photomultiplier tubes (PMTs). States |1⟩ and |2⟩ have identical first-order Zeeman shifts so the two-photon resonance is maintained across the trapped atom clouds. Cold atoms and co-propagating lasers eliminate Doppler effects. However, off-resonance transitions to state |4⟩ prevent perfect transmission of the light pulses in this case.

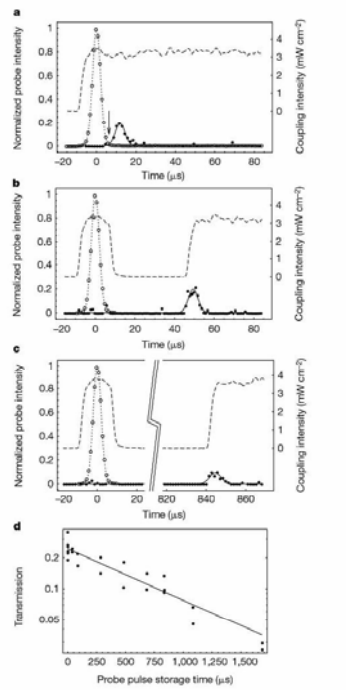

Figure 2 Measurements of delayed and revived probe pulses. Open circles (fitted to the dotted gaussian curves) show reference pulses obtained as the average of 100 probe pulses recorded in the absence of atoms. Dashed curves and filled circles (fitted to the solid gaussian curves) show simultaneously measured intensities of coupling and probe pulses that have propagated under EIT conditions through a 339-μm-long atom cloud cooled to 0.9 μK. The measured probe intensities are normalized to the peak intensity of the reference pulses (typically, $\Omega_p/\Omega_c = 0.3$ at the peak). **a**, Probe pulse delayed by 11.8 μs. The arrow at 6.3 μs indicates the time when the probe pulse is spatially compressed and contained completely within the atomic cloud. (The intersection of the back edge of the reference pulse and the front edge of the delayed pulse defines a moment when the tail of the probe pulse has just entered the cloud and the leading edge is just about to exit.) **b**, **c**, Revival of a probe pulse after the coupling field is turned off at $t = 6.3$ μs and turned back on at $t = 44.3$ μs and $t = 839.3$ μs, respectively. During the time interval when the coupling laser is off, coherent information imprinted by the probe pulse, is stored in the atomic medium. Upon subsequent turn-on of the coupling field, the probe pulse is regenerated through coherent stimulation. The time constants for the probe and coupling PMT amplifiers are 0.3 μs and 3 μs, respectively. The actual turn on/off time for the coupling field is 1 μs, as measured with a fast photodiode. **d**, Measured transmission of the probe pulse energy versus storage time. The solid line is a fit to the data, which gives a 1/e decay time of 0.9 ms for the atomic coherence.

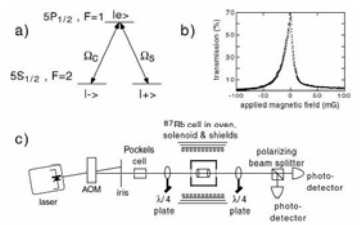

FIG. 1. (a) Λ-type configuration of ^{87}Rb atomic states resonantly coupled to a control field (Ω_c) and a signal field (Ω_s). (b) A typical observed Rb Faraday resonance in which the transmission intensity is shown as a function of magnetic field (i.e., detuning of Zeeman levels from the two-photon resonance condition). The full width of this resonance is about 30 mG which corresponds to a 40 kHz level shift. (c) Schematic of the experimental setup.

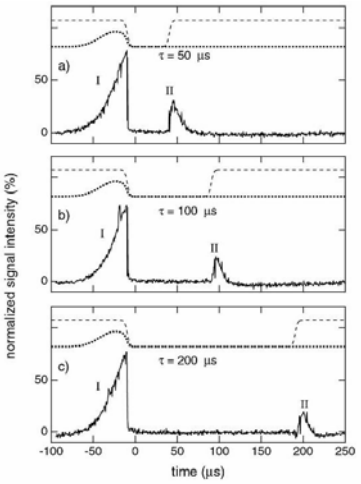

FIG. 2. Observed light pulse storage in a ^{87}Rb vapor cell. Examples are shown for storage times of (a) 50 μs, (b) 100 μs, and (c) 200 μs. (Background transmission from the control field, which leaks into the signal field detection optics, has been subtracted from these plots.) Signals are normalized to the peak intensity of the light transmitted through the stationary EIT medium. Shown above the data in each graph are calculated representations of the applied control field (dashed line) and input signal pulse (dotted line). Estimated peak $\Omega_c \sim 3$ MHz, $\Omega_s \sim 0.9$ MHz, and $\sqrt{\kappa} \sim 2000$ MHz.

Atoms – L: Scl

Slow Light

L. Hau et al. Nature **397**, 594 (1999).

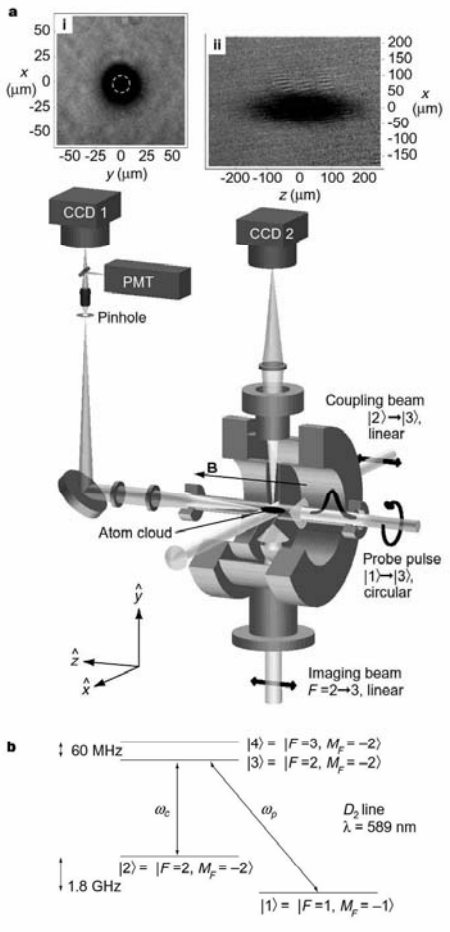

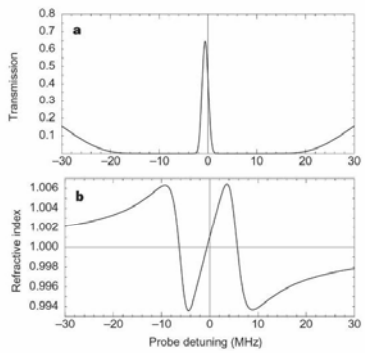

Figure 2 Effect of probe detuning. **a**, Transmission profile. Calculated probe transmission as a function of detuning from the $|1\rangle \rightarrow |3\rangle$ resonance for an atom cloud cooled to 450 nK, with a peak density of 3.3×10^{12} cm^{-3} and a length of 229 μm (corresponding to the cloud in inset (ii) of Fig. 1a). The coupling laser is resonant with the $|2\rangle \rightarrow |3\rangle$ transition and has a power density of 52 mW cm^{-2}. **b**, Refractive index profile. The calculated refractive index is shown as a function of probe detuning for the same parameters as in **a**. The steepness of the slope at resonance is inversely proportional to the group velocity of transmitted light pulses and is controlled by the coupling laser intensity. Note that as a result of the a.c. Stark shift of the $|2\rangle \rightarrow |3\rangle$ transition, caused by a coupling of states |2⟩ and |4⟩ through the coupling laser field, the centre of the transmission and refractive index profiles is shifted by 0.6 MHz. The shift of the refractive index profile results in the nonlinear refractive index described in the text.

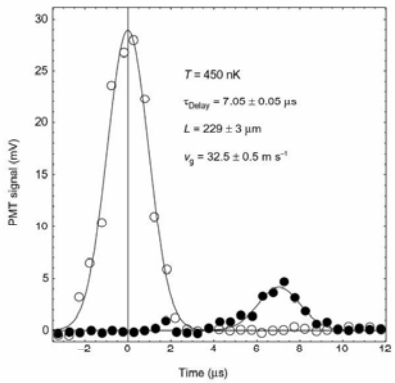

Figure 3 Pulse delay measurement. The front pulse (open circles) is a reference pulse with no atoms in the system. The other pulse (filled circles) is delayed by 7.05 μs in a 229-μm-long atom cloud (see inset (ii) in Fig. 1a). The corresponding light speed is 32.5 m s^{-1}. The curves represent gaussian fits to the measured pulses.

Chinmeshwar, A. Rauschenbeutel